SAPIENZA
UNIVERSITÀ DI ROMA

PhD in Biochemistry, XXIX Cycle (A.A. 2013/2016)

Different approaches to optimize the antimicrobial properties of cationic peptides: substitution by non-coded amino acids and conjugation to nanoparticles.

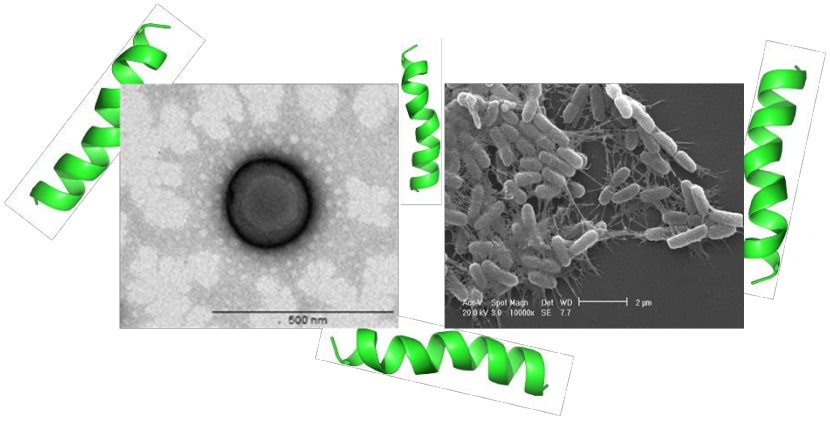

Tutor: Prof. Maria Luisa Mangoni

Coordinator: Prof. Francesco Malatesta

PhD student

Bruno Casciaro

Index

List of papers relevant for this thesis

- **Casciaro B**., Moros M., Rivera-Fernandez S., Bellelli A., de la Fuente J., and Mangoni ML. "**Gold-nanoparticles coated with the antimicrobial peptide esculentin-1a(1-21)NH_2 as a reliable strategy for antipseudomonal drugs"** Acta Biomater. (2016) Sep 29. pii: S1742-7061(16)30514-1. doi: 10.1016/j.actbio.2016.09.041

- Biondi B., **Casciaro B**., di Grazia A., Cappiello F., Luca V., Crisma M. and Mangoni ML. "**Effects of Aib residues insertion on the structural-functional properties of the frog skin derived peptide esculentin-1a(1-21)-NH_2**". Amino Acids (2016) Oct 11

- Di Grazia A, Cappiello F, Cohen H, **Casciaro B**, Luca V, Pini A, Di YP, Shai Y, Mangoni ML. "**D-Amino acids incorporation in the frog skin-derived peptide esculentin-1a(1-21)NH_2 is beneficial for its multiple functions**". Amino Acids. (2015) Dec; 47(12):2505-19. doi: 10.1007/s00726-015-2041-y

- d'Angelo I, **Casciaro B**., Miro A, Quaglia F, Mangoni ML, Ungaro F. "**Overcoming barriers in *Pseudomonas aeruginosa* lung infections: Engineered nanoparticles for local delivery of a cationic antimicrobial peptide**". Colloids Surf B Biointerfaces. 2015 Aug 22; 135:717-725. doi: 10.1016/j.colsurfb.2015.08.027

List of other papers

- Mangoni ML, Di Grazia A, Cappiello F, **Casciaro B**, Luca V. "**Naturally Occurring Peptides from Rana temporaria: Antimicrobial Properties and More**". Curr Top Med Chem. 2016;16(1):54-64.

- Tabbene O, Azaiez S, Di Grazia A, Karkouch I, Ben Slimene I, Elkahoui S, Alfeddy MN, **Casciaro B**, Luca V, Limam F, Mangoni ML. "**Bacillomycin D and its combination with amphotericin B: promising antifungal compounds with powerful antibiofilm activity and wound healing potency**". J Appl Microbiol. 2015 Dec 16. doi: 10.1111/jam.13030

- Tabbene O, Di Grazia A, Azaiez S, Ben Slimene I, Elkahoui S, Alfeddy MN, **Casciaro B**, Luca V, Limam F, Mangoni ML. "**Synergistic fungicidal activity of the lipopeptide bacillomycin D with amphotericin B against pathogenic Candida species**". FEMS Yeast Res. 2015 Jun; 15(4):fov022. doi: 10.1093/femsyr/fov022.

- Di Giampaolo A, Luzi C, **Casciaro B**, Bozzi A, Mangoni ML, Aschi M. "**The P-113 peptide: new experimental evidences on its biological activity and conformational insights from Molecular Dynamics simulations**". Biopolymers. 2014 Mar; 102(2):159-67. doi: 10.1002/bip.22452.

Research is what I'm doing when I don't know what I'm doing.

(Cit. Wernher von Braun)

1. Introduction

1.1 – ANTIMICROBIAL PEPTIDES: GENERAL FEATURES AND INNATE IMMUNITY

Antimicrobial peptides (AMPs) are evolutionally conserved molecules found in bacteria, fungi as well as in higher eukaryotes (Nakatsuji and Gallo 2012), (Ageitos, Sanchez-Perez et al. 2016), and act as an immediate host response to a wide spectrum of microorganisms, before the adaptive immune system is activated (Pasupuleti, Schmidtchen et al. 2012). In mammals, AMPs are generally synthesized in tissues exposed to the external environment, such as the skin, the intestine, the lungs and the circulating white cells. AMPs are encoded by genes, ribosomally synthesized as pre-propeptides of 60-170 amino acids, and then processed by different kind of proteases to the active mature peptides. The innate immune system can respond in a matter of hours before the adaptive immunity is activate. Indeed, the time needed to synthesize and process a pre-propeptide is certainly shorter than the time required to produce two heavy and two light immunoglobulin chains, the production of which also requires the differentiation of a memory cell to a plasma cell. This prompt response is very important considering the difference in the growth rate between a bacterium (generation time 20-30 min) and a lymphocyte (24-48 hours of doubling time). In addition, another advantage of AMPs as key molecules of the innate immunity is that they can function without high specificity (Boman 1995).

AMPs expression can be constitutive or inducible upon inflammation or infection through a Toll-like receptor-mediated signaling transduction cascade. This pathway can be triggered by microbial components (e.g. lipopolysaccharides,

LPS) and leads to the activation of NF-kB-controlled genes, including those encoding for AMPs (Thaiss, Levy et al. 2016).

Recently, in addition to their antimicrobial activity, AMPs from higher eukaryotes have been found to act as intracellular signaling molecules and to coordinate the innate and adaptive host defense responses (Hemshekhar, Anaparti et al. 2016), influencing processes like: (i) cytokine release (Afacan, Yeung et al. 2012); (ii) immune cell differentiation (Davidson, Currie et al. 2004); (iii) chemotactic activity (Mookherjee and Hancock 2007); wound-healing and angiogenesis (Wu, Wong et al. 2010). Some of these properties would be considered pro-inflammatory, but AMPs actually can suppress TLR signaling responses, by blocking the LPS-stimulated production of cytokines, such as the tumor necrosis factor-alpha (TNF-α). This would hamper the emergence of septic shock syndrome in animal models (Bowdish and Hancock 2005; Hancock and Sahl 2006).

1.2 – STRUCTURAL PROPERTIES

AMPs generally are low molecular weight molecules (2-50 kDa) although some of them have a larger size (Brogden, Ackermann et al. 2003).

According to their secondary structures, AMPs can be classified into the following four groups (Boman 1995), (Powers and Hancock 2003):

Group I: linear peptides with α-helical structure [Fig. 1A], such as magainin, the cathelicidin LL37 and cecropin (Huang, Huang et al. 2010);

Group II: peptides consisting of β-strands connected by one or more intramolecular disulfide bridges [Fig. 1B], such as defensins and protegrins (Taylor, Barran et al. 2008);

Group III: linear peptides with an extended structure [Fig. 1C] and a high proportion of one or more residues (proline, tryptophan, arginine) such as indolicidin and bactenecins (Chan, Prenner et al. 2006);

Group IV: peptides exhibiting a hairpin-loop structure [Fig. 1D], that is interconnected by at least one disulfide bridge. An example is given by thanatin (Ma, Niu et al. 2016).

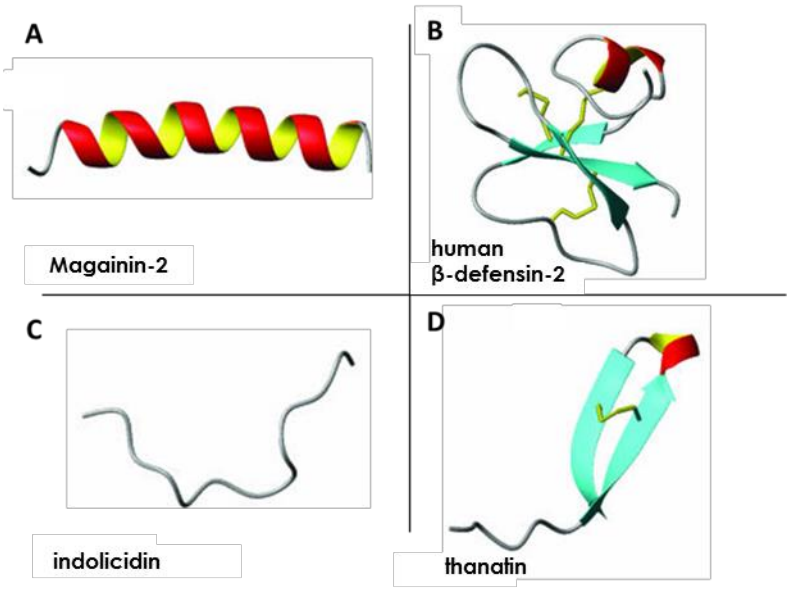

Figure 1 - Representative secondary structures of AMPs [modified by (Jenssen 2009)]

1.3 – AMPs: MECHANISM OF ACTION

The most common AMPs in nature are those with an α-helix or a β-sheet conformation (Powers and Hancock 2003) and α-helical peptides are among the most studied AMPs to date. Based on their mechanism of microbicidal activity, AMPs can be divided into two classes: membranolytic peptides and non-membrane active peptides.

With reference to the first group, the most predominant AMPs have an α-helical conformation upon interaction with biological membranes (Sato and Feix 2006) [Fig. 2].

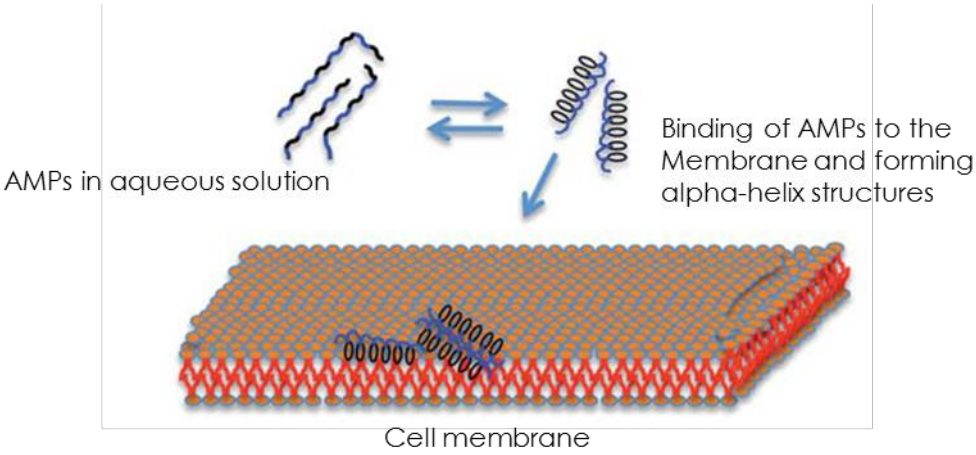

Figure 2 - Schematic model of the interaction of α-helix AMPs with the cell membrane (modified by Huerta-Cantillo 2016)

Looking at the various amino acid sequences of AMPs, their interactions with the membrane cannot be predicted: indeed, it depends on a

combination of biochemical/biophysical features, including the size, the cationicity, the distribution of cationic residues, the amphiphilic character and oligomeric state (Hall and Aguilar 2010). However, before reaching the target microbial membrane, AMPs interact with the negatively charged components of the microbial cell surface, such as LPS, in the outer membrane of Gram-negative bacteria, or teichoic acids in the peptidoglycan layer of Gram-positive bacteria [Fig. 3].

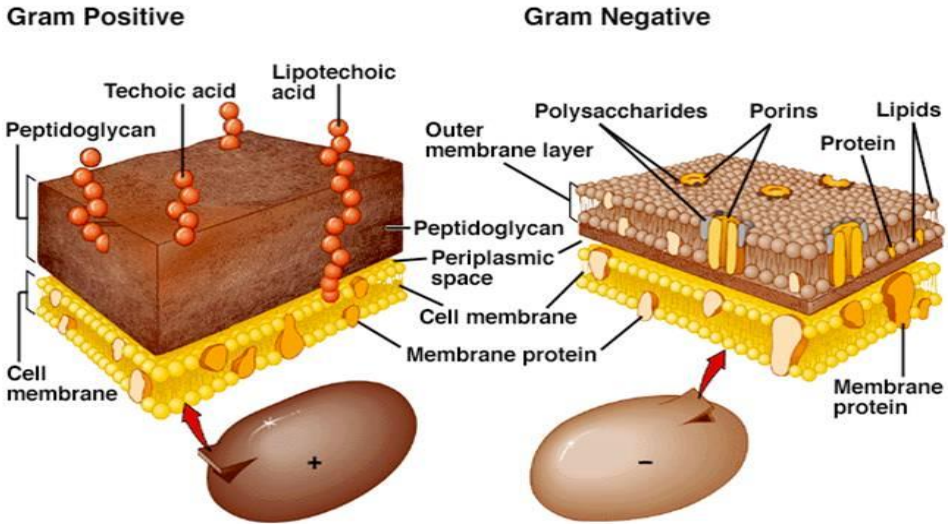

Figure 3 - Schematic representation of the cell wall of Gram-positive and Gram-negative bacteria

Once reached the periplasmic space, AMPs target the plasma membrane, which is rich in anionic lipids and perturb it, following one of these mechanisms:

- **Barrel-stave model**, in which AMPs are inserted perpendicularly to the plane of the membrane bilayer (Ehrenstein and Lecar 1977), forming a pore like a stave (Zhang, Rozek et al. 2001). In this structure, the hydrophobic surfaces of the helices interact with the fatty acid chains of the membrane phospholipids, while the hydrophilic surfaces point inward, producing a transmembrane pore. Progressive recruitment of additional peptide monomers leads to an increase of the pore size. The leakage of intracellular components through these pores subsequently causes cell death [Fig. 4A]. It should be noted that a transmembrane pore can be formed from as few as three molecules. Therefore, peptides that act via the barrel-stave mechanism should kill bacteria about thousand fold below the experimentally determined micromolar concentrations.

- **Toroidal pore model** that resembles the "barrel-stave" model. However, according to this model, AMPs are always in contact with phospholipid head groups [Fig. 4C] (Brogden 2005) of the membrane, even when they are perpendicularly inserted into the lipid bilayer. The polar faces of the peptides associate with the polar head groups of the lipids. The lipids in these openings then tilt from the normal position and connect the two leaflets of the membrane, forming a continuous bend from the top to the bottom in the fashion of a toroidal hole. The pore is lined by both the

peptides and the lipid head groups, which are likely to screen and mask cationic peptide charges.

- **Disordered toroidal pore model** in which pore formation is more stochastic and involves fewer peptides (Sengupta, Leontiadou et al. 2008).

- **Membrane thinning/thickening affection model,** in which the thickness of the bilayer can be affected by the presence of the peptides, or the membrane itself can be remodeled to form domains rich in anionic lipids surrounding the peptide.

- **Carpet-like model**, in which the peptide molecules line parallel to the membrane surface via electrostatic interactions and cover it in a "carpet"-like manner [Fig. 4B]. In the second step, the peptides reorient themselves such that their hydrophobic face is toward the lipids and the hydrophilic face toward the phospholipid head-groups. After a threshold concentration has been reached, the peptides cause membrane permeation, which depends upon the properties of a particular peptide. Practically, independently of the type of the permeation pathways, which are described as toroidal pores or channel aggregates, higher peptide concentrations can lead to membrane disintegration (membrane packing collapses into fragments with physical disruption of the microbial cell) (Shai 2002).

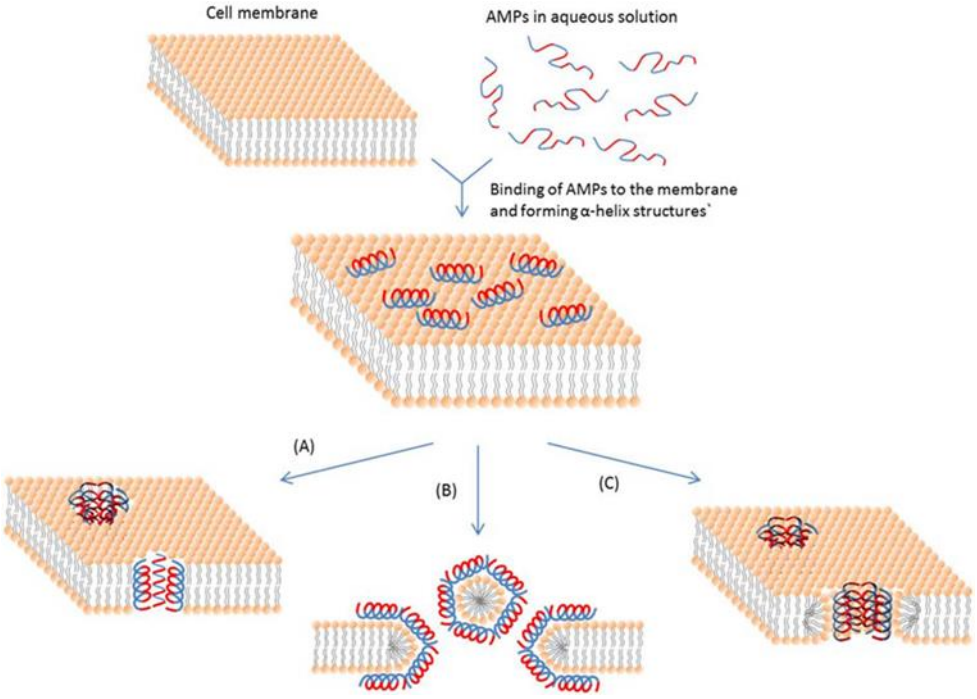

*Figure 4 - Schematic representation of some mechanisms of action of membrane-active AMPs: barrel-stave model (**A**), carpet-like model (**B**) and toroidal-pore model (**C**). The hydrophobic portions of AMPs are in blue, while the hydrophilic ones are in red [From (Bahar and Ren 2013)].*

With reference to the second group (i.e. non-membrane active AMP), the mechanism of action of AMPs can involve the inhibition of intracellular processes, such as (i) synthesis of nucleic acids; (ii) synthesis of proteins or enzymatic activity; (iii) synthesis of the cell wall or microbial septum formation (Nguyen, Haney et al. 2011).

One of the reasons accounting for the preferential activity of AMPs towards microbial cells is linked to the anionic nature of microbial membranes that are predominantly composed of phosphatidylethanolamine (PE) phosphatidylglycerol (PG) and cardiolipin (CL), with a high transmembrane potential (-140 mV). In contrast, the outer surface of mammalian cell membranes is composed predominantly of zwitterionic lipids such as phosphatidylcholine (PC) and sphingomyelin, which do not bind strongly to the positively-charged AMPs. This hypothesis is supported by *in vitro* studies on the interaction between AMPs and artificial vesicles made of different lipids. These studies suggest that the selectivity of AMPs for prokaryotic cells is associated to their higher affinity for bacterial membranes compared to normal mammalian cell membranes [Fig. 5].

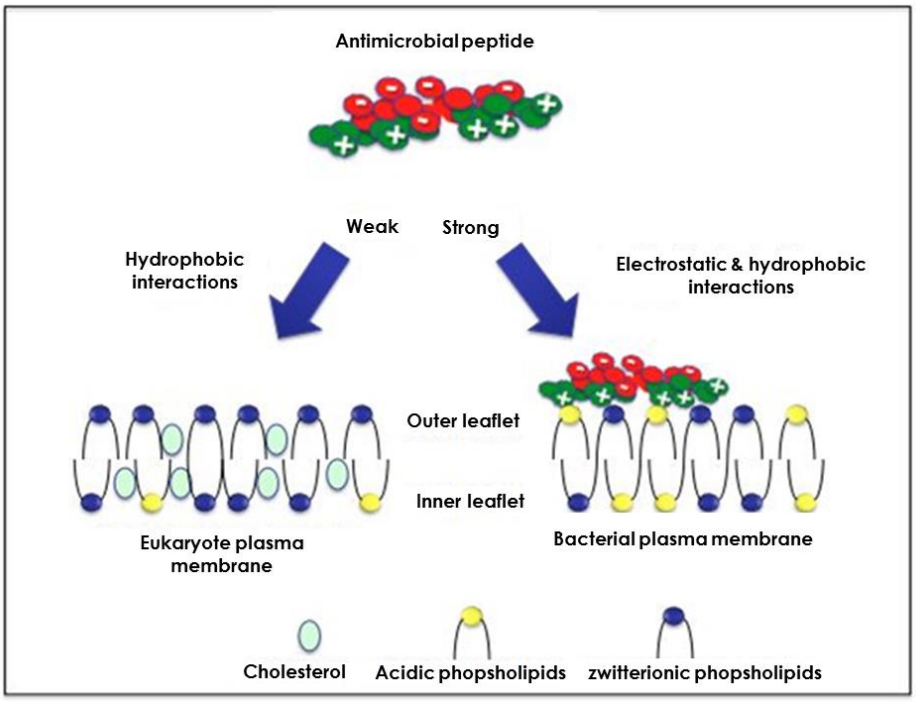

Figure 5 - Molecular basis of cell selectivity of AMPs. AMPs form amphipathic structures with a positively charged face (green) and a hydrophobic face (red). Electrostatic interaction between the positive charges of AMPs and negatively charged components (yellow) at the eukaryotic cell surface (left) and bacterial surface (right) is the major driving force for cellular association.

However, the *in vitro* interactions between AMPs and membranes are not always superimposable to those observed *in vivo*. An example is given by the human cathelicidin AMP LL-37: despite its high affinity for model membranes of bacterial-like composition (Neville, Cahuzac et al. 2006), its *in vivo* antimicrobial activity is largely restricted, presumably due to physiological conditions (Bowdish, Davidson et al. 2005).

1.4 –PHYSICOCHEMICAL PROPERTIES OF ANTIMICROBIAL PEPTIDES

The interaction of AMPs with a membrane and their target cell selectivity are the result of a combination of multiple physicochemical factors such as the AMP's structure, size, net charge, hydrophobicity and amphipathicity (Zelezetsky and Tossi 2006). Changing these properties, would help to modify the spectrum of activity of AMPs as well as their potency, according to what reported below:

- **Length**: To form an amphipathic structure with hydrophobic and hydrophilic faces, at least 7-8 amino acids are needed. The minimal length to span a phospholipid bilayer for α-helical AMPs is about 20-22 amino acids; however, the peptide's length can affect the AMP's cytotoxicity. A shorter length is often associated to a lower cytotoxicity. Some examples are provided by: (i) a shortened version of melittin, the 15-residues-fragment of its C-terminal (Subbalakshmi, Nagaraj et al. 1999) and (ii) a shorter derivative of HP(2-20), derived from N-terminus of *Helicobacter pylori* Ribosomal protein L1 (RpL1) (Park, Park et al. 2007). Both peptides exhibited at least 300-fold lower toxicity to rat and human erythrocytes, respectively, compared to their original forms. Therefore, AMPs' length should be taken into consideration when designing new synthetic peptides.

- **Net charge**: AMPs' net charge is the sum of all positive and negative charges of ionizable groups. Cationicity results to be the main factor for initial electrostatic interaction with the negatively-charged microbial membranes. Altering the net charge, AMPs' activity and cytotoxicity can be changed to achieve a selective microbial killing with minimized toxic effects (Jiang, Vasil et al. 2009).

- **Hydrophobicity and amphipathicity**: Generally, almost 50% of amino acids in the primary structure of natural AMPs are hydrophobic. Importantly, an increased hydrophobicity of AMPs can increase their cytotoxicity (Dathe, Wieprecht et al. 1997) while decreasing their antimicrobial efficacy (Lee, Kim et al. 2002). However, a study conducted by Fernandez-Vidal and co-workers (Fernandez-Vidal, Jayasinghe et al. 2007) showed that amphipathicity is more important than hydrophobicity for the binding and permeation of microbial membranes.

- **Helicity**: The ease of α-helix formation and stability are important parameters for the perturbation of biological membranes (Liu, Fang et al. 2011). In particular, a reduction in the helical content of a peptide has been found to significantly weaken its interaction with zwitterionic phospholipid bilayers (Andrushchenko, Vogel et al. 2007). On the other hand, a stabilized α-helical structure has been

found to enhance the antimicrobial activity of AMPs against Gram-positive bacteria and fungi (Giangaspero, Sandri et al. 2001).

1.5 – FROG-SKIN ANTIMICROBIAL PEPTIDES

Amphibian skin is a rich source of biologically active compounds that are assumed to have diverse physiological and defense functions (Conlon 2011). Frog-skin AMPs are synthesized at low metabolic cost by dermal serous glands, which are mainly located in the dorsal region of the animal and are controlled by sympathetic axons. The cytoplasm of the cells is rich in granules where AMPs are stored, and the lumen is reduced to a small empty cavity. Contraction of myocytes surrounding the glands, as a reaction to stress or tissue damage, causes a synchronous discharge of their content, in a holocrine mechanism (Konig, Bininda-Emonds et al. 2015).

A large number of AMPs have been isolated and identified from amphibian families belonging to the species *Xenopus laevis*, *Bombina variegata*, *Bombina orientalis, Phyllomedusa bicolor* and *Phyllomedusa sauvagei* and different species of *Rana* (Ladram and Nicolas 2016) [see Tab. 1].

Table 1 - Primary structures of some naturally occurring frog-skin AMPs or their derivatives.

Peptide	Sequence
Brevinin-1E	**FLPLLAGLAANFLPKIFCKITRKC**
Brevinin-1Lb	**FLPMLAGLAASMVPKFVCLITKKC**
Magainin-1	**GIGKFLHSAGKFGKAFVGEIMKS**
Magainin-2	**GIGKFLHSAKKFGKAFVGEIMNS**
esculentin-1	**GIFSKLGRKKIKNLLISGLKNVGKEVGMDVVRTGIDIAGCKIKGEC**
esculentin-1a	**GIFSKLAGKKIKNLLISGLKNVGKEVGMDVVRTGIDIAGCKIKGEC**
esculentin-1b	**GIFSKLAGKKLKNLLISGLKNVGKEVGMDVVRTGIDIAGCKIKGEC**
esculentin-C	**CGIFSKLAGKKLKNLLISGLKNVGKEVGLDVVRTGIDIAGCKIKGECM**
esculentin-2a	**GILSLVKGVA KLAGKGLAKE GGKFGLELIA CKIAKQC**
Esc(1-18)	**GIFSKLAGKKLKNLLISG-NH_2**
Esc(1-21)	**GIFSKLAGKKIKNLLISGLKG-NH_2**

From various *Rana* genera, many AMPs have been isolated and identified with common features and structures. They have been classified into several families encompassing brevinin-1, brevinin-2, nigrocin, temporin, esculentin-1 and esculentin-2.

1.5.1 – The esculentin-1 family

All members of this family are 46-amino acid residues long and contain a C-terminal hepta-membered ring stabilized by a disulfide bridge

They have a net charge of +5 at neutral pH and an amphipathic α-helical structure in membrane mimetic environments (Wang, Zhang et al. 2016). Various members belonging to the esculentins-1 family were isolated and purified from the cutaneous secretions of *Pelophylax lessonae/ridibundus* (previously classified as *Rana esculenta*) specimen [Fig. 6], using reversed-phase high performance liquid chromatography.

Figure 6 - A specimen of Pelophylax lessonae/ridibundus

The antimicrobial activity of these peptides against several microbial strains and their hemolytic activity on human erythrocytes are reported in [Tab. 2] and expressed as lethal concentration as reported in (Simmaco, Mignogna et al. 1993).

Table 2 - Antimicrobial and lytic activity of two esculentin peptides. ND= not determined

Strains	Lethal concentration*(μM)	
	Esculentin-1	**Esculentin-C**
Escherichia coli D21	0.2	0.2
Bacillus megaterium Bm11	0.1	0.1
Staphylococcus Cowan I	0.4	0.4
Pseudomonas aeruginosa ATCC15692	0.7	1.4
Candida albicans	0.5	ND
Red blood cells	>100	ND

*Values taken from (Simmaco, Mignogna, et al. 1993) and (Mangoni, Fiocco et al. 2003)

Interestingly, a fragment corresponding to the 19-46 portion of esculentin peptides was also isolated from skin secretions.

It was devoid of antimicrobial activity, presumably due to its low net positive charge (+1 versus +5 of the whole molecule) at neutral pH (Simmaco, Mignogna et al. 1994). Since no antimicrobial activity was detected for this fragment, it was then investigated whether this activity was retained in the N-terminal portion of the esculentin-1 peptide. The 1-18 fragment was not found in the HPLC fractionation of the secretion, possibly because of its proteolytic degradation. Therefore, its antimicrobial activity was analyzed in detail on a synthetic peptide, Esc(1-18), amidated at the C-terminus [Tab. 1] to maintain a net charge

of +5 at neutral pH and to increase its stability (Mangoni, Fiocco et al. 2003). Note that the amidation at the carboxyl-end is a very common post-translational modification in linear AMPs from frog skin (Mangoni, Papo et al. 2006), (Nicolas and El Amri 2009).

It was found that Esc(1-18) adopted an α-helical structure in lipid vesicles mimicking the anionic character of microbial membranes and that its antimicrobial activity was comparable to that of the full-length peptide (with lethal concentration values ranging from 0.1 to 1.5 μM). Furthermore, it showed a lower hemolytic capacity compared to the full-length peptide (Mangoni, Fiocco et al. 2003).

Since the minimum length for a peptide in α-helical conformation to span a phospholipid bilayer is about 20 amino acids, a longer analog containing 21 residues and amidated at its C-terminus, named esculentin-1a(1-21)NH_2, [Tab. 1, Esc(1-21)], was further synthesized and analyzed for its antimicrobial activity.

1.5.2 – Esculentin-1a(1-21)NH_2, Esc(1-21)

Esculentin-1(1-21)NH_2, Esc(1-21), shares the first 20 residues with the natural esculentin-1a plus a glycinamide at its C-terminus [Tab. 1] (Islas-Rodriguez, Marcellini et al. 2009). Differently from Esc(1-18), Esc(1-21) carries the substitution Leu-11-Ile and three additional C-terminal residues (Leu-Lys-Gly) which give it a higher net positive charge at neutral pH (+6); an important property for the electrostatic interaction with the negatively-charged membranes of microbial cells.

It has been demonstrated that Esc(1-21) has a potent antimicrobial activity mainly against Gram-negative bacteria, e.g. *Pseudomonas aeruginosa* including both free-living and sessile forms of this microbial pathogen (Luca, Stringaro et al. 2013). Esc(1-21) displayed the same efficacy against reference and clinical isolates of *P. aeruginosa* with a rapid bactericidal activity (15 min), regardless of their multi-drug resistance or mucoid phenotype. This is indicated by the similar minimal peptide concentration which inhibits microbial growth (MIC) of these strains (4 μM) as well as by the comparable bactericidal concentration causing 99.9% killing of these strains (0.5 μM or 1 μM) (Luca, Stringaro et al. 2013). In comparison, a weaker activity was detected against Gram-positive bacterial strains with MIC values ranging from 1 μM to 64 μM (Kolar, Luca et al. 2015).

Furthermore, Esc(1-21) was found to have the capacity to promote re-epithelialization of an injured area produced in a monolayer of keratinocytes, the most abundant cells in epidermis (Haslam, Roubos et al. 2014), at a faster rate than the mammalian AMP LL-37 (Di Grazia, Cappiello et al. 2015).

1.6 – *PSEUDOMONAS AERUGINOSA*

P. aeruginosa [Fig. 7] is an opportunistic Gram-negative bacterium causing life-threatening infections such as keratitis, pneumonia and burn wounds skin infections (Gellatly and Hancock 2013).

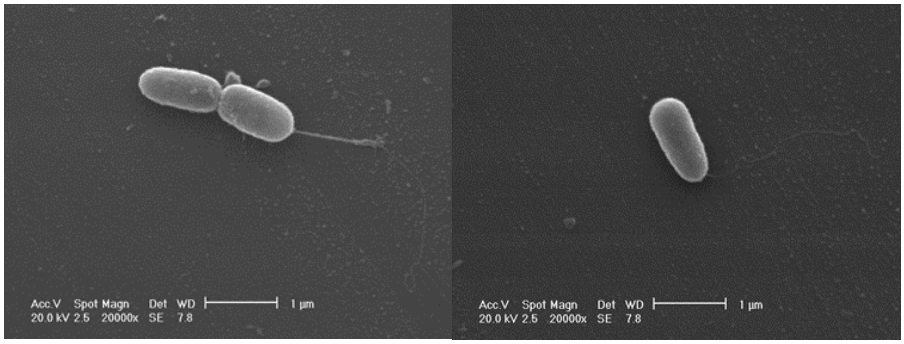

Figure 7 - Pseudomonas aeruginosa free-living cells

Its adaptability and high intrinsic antibiotic resistance enable it to survive in a wide range of natural and artificial settings, including abiotic and biological surfaces. The strengths of this bacterium reside in its high production of virulence factors and the ability to form biofilm causing direct damage to host tissues or increasing the bacterium competitiveness (Streeter, Neuman et al. 2016). *P. aeruginosa* biofilms [Fig. 8] are bacterial communities embedded in a self-produced matrix of extracellular polymeric substances, which confer them a greater resistance to physical and chemical factors, including conventional antibiotics, and to immune cells, favoring colonization of nearby surfaces [Fig. 8] (Flemming, Wingender et al. 2016).

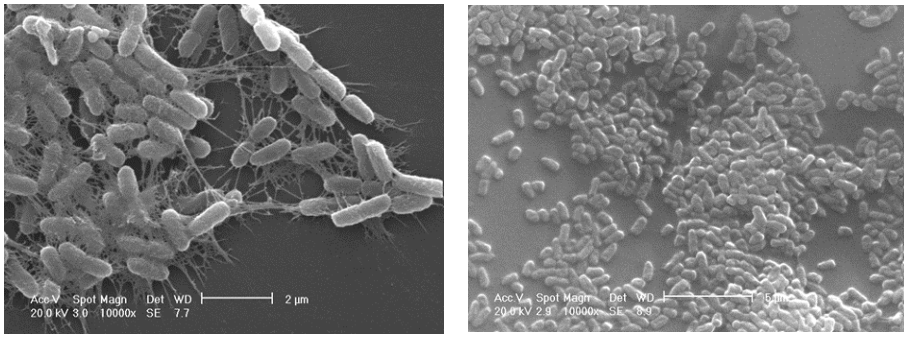

Figure 8 - Pseudomonas aeruginosa biofilm communities

P. aeruginosa infections are often associated with compromised host defenses e.g. neutropenia, severe burns or cystic fibrosis (CF) (Lyczak, Cannon et al. 2000). In the latter case, *P. aeruginosa* colonizes the mucus present in the airways of CF patients causing persistent and resistant bacterial infections that conventional antibiotics cannot eradicate. AMPs may represent a breakthrough in the treatment of resistant infections because of their non-specific mechanism of action, which involves the membrane disruption.

1.7 – ANTIMICROBIAL PEPTIDES AS DRUGS: LIMITATIONS AND POSSIBLE MODIFICATIONS

In the last decades, several peptides have entered clinical trials as antimicrobial or/and immunomodulatory drugs [e.g. in Tab. 3] (Velden, van Iersel et al. 2009), (Paquette, Simpson et al. 2002), (Melo, Dugourd et al. 2006), (Nilsson, Janson et al. 2015).

Table 3 - Some examples of AMPs tested in clinical studies

Peptide name	Parent name	Outcome
hLF1-11	Lactoferrin	established safety in humans
P-113	Histatins	Safety with reduction in gingivitis and gingival bleeding
Omiganan	Indolicidin	Effective for killing bacteria that live on the surface of the skin
Omiganan	Indolicidin	Reduced catheter infections
LL-37	Cathelicidin	Approved, no yet recruiting
Talactoferrin	Lactoferrin	Completed, no results posted

In spite of their important natural roles, several limitations can hinder the development of AMPs as therapeutics:

- Toxicity against mammalian cells at therapeutic dosages;
- Poor pharmacokinetics due to degradation by proteolytic enzymes;
- Hampered delivery to the target site at effective concentrations.

Recent research on AMPs has focused on methods to overcome these drawbacks without causing a significant reduction in their antimicrobial efficacy (Fjell, Hiss et al. 2012). Amino acid substitution is one of the applied strategies for AMP modification. Below is a list of the most common approaches to optimize the biological properties of AMPs:

- **Modification of AMPs by different natural amino acids**: most of these studies focus on certain amino acids due to their unique properties. For example, proline shows low propensity to form α-helical structures; thus,

changes in the proline content may lead to alteration of the peptide conformation with a resulting reduction in the cytotoxicity (Zhang, Benz et al. 1999). Furthermore, the addition of positively-charged residues into the primary structure of AMPs can also reduce the cytotoxicity. An example is given by the peptide P60.4, an analog of the human LL-37 with two basic residues in substitution of two neutral ones. This analog has been successfully used in nasal application against methicillin-resistant *Staphylococcus aureus* (MRSA) (Goblyos, Schimmel et al. 2013).

- **Modification of AMPs by amidation:** it has been demonstrated that the amidation at the carboxyl end of a peptide results in a more stable and active AMP, due to the higher cationicity. As shown by Kim et al., the C-terminal amidation of the AMP PMAP-23 increased by almost 10-fold the peptide cellular uptake, its interaction and perturbation of bacterial membranes with respect to the unmodified AMP (Kim, Park et al. 2011).

- **Modification of AMPs by non-coded amino acids:** this approach is widely used in biochemistry to modify native AMPs. For example, the incorporation of β-didehydrophenylalanine [Fig. 9] in the primary structure of VS1 increases the resistance to proteolytic degradation. β-didehydrophenylalanine is an unnatural amino acid used to provide better folding properties to AMPs (Gupta and Chauhan 2011), (Torino, Mollica et al. 2010).

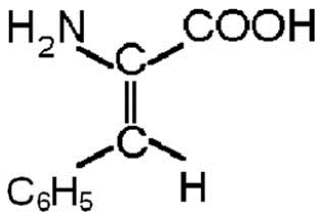

Figure 9 - Chemical stucture of β-didehydrophenylalanine residue

Another type of non-natural amino acid mainly used to increase the stability of α-helix conformation and presumably the spectrum of activity of AMPs, is the α-aminoisobutyric acid (Aib) [Fig. 10], (Bellanda, Peggion et al. 2001), (De Zotti, Biondi et al. 2012).

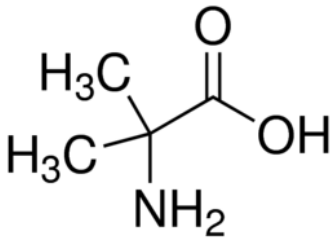

Figure 10 - Chemical structure of α-aminoisobutyric acid (Aib) residue

An important strategy that is often used to reduce AMPs cytotoxicity without negative effects on the peptide's functionality is the substitution of L-amino acids with the corresponding D-enantiomers. However, D-amino acids incorporation can also modify the AMPs' antimicrobial activity and selectivity. Furthermore, D-amino acids-containing analogues are highly resistant to proteolytic degradation, making AMPs more tolerant to proteases (Giuliani and Rinaldi 2011).

- **Design of hybrid peptides:** this is another innovative strategy to enhance the spectrum of activity of AMPs and to reduce their hemolytic activity. It consists in the fusion of two peptides with antimicrobial activity but directed to a different target (Acuna, Picariello et al. 2012). An example is given by the HDB2/HDB3-chimera peptide corresponding to the fusion of the two different human β-defensin-2 (HDB2) and human β-defensin-3 (HDB3) that act against different microorganisms. The resulting chimera showed the combined antimicrobial activities of the individual peptides (Spudy, Sonnichsen et al. 2012).

- **Design of antimicrobial peptide conjugates.** This novel strategy includes the synthesis of stabilized AMPs, AMPs congeners, immobilized AMPs and AMP conjugates (Brogden and Brogden 2011). In fact, AMPs can be attached/incorporated to/into nano-micro systems (e.g. nanoparticles) to improve their biostability, to enhance their antimicrobial activity and to reach the infection sites. Engineered nanoparticles (NPs) represent an innovation in the field of diagnostics and biomedicine. They can be produced with various materials to obtain NPs of different size, shape and surface properties suitable for different therapeutic approaches (Yih and Al-Fandi 2006).

  In recent years, as for conventional antibiotics, scientific research has focused on the realization of AMP-nano conjugates. This is proved by the increasing number of scientific reports (Soica, Coricovac et al. 2016) that show the use of biodegradable materials, such as poly(lactic-co-glycolic acid) (PLGA) [Fig. 11] (Gutjahr, Phelip et al. 2016) or inorganic particles

(such as gold or silver) for new therapeutic formulations (Rai, Pinto et al. 2016), (Ramesh, Grijalva et al. 2016), (Ali, Zafar et al. 2016).

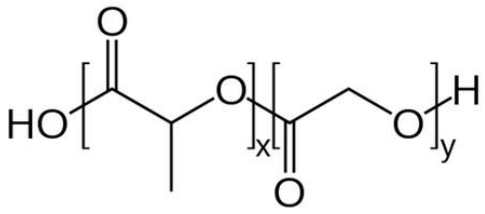

Figure 11 - Chemical structure of PLGA

Encapsulation of drugs into biodegradable NPs is becoming one of the innovative strategies for drug delivery, such as the formulation of inhalable powder for treatment of lung infections (d'Angelo, Conte et al. 2014). The encapsulation should serve (i) to protect the drug, i.e. peptide, from the action of proteolytic enzymes; (ii) to assist the drug delivery to the target site at high concentrations and (iii) to prolong the drug residence time *in situ*, thus sustaining its pharmacological effect and reducing the number of administrations (d'Angelo, Conte et al. 2015), (d'Angelo, Quaglia et al. 2015). The first two above-mentioned objectives can also be achieved by the conjugation of the compound to inorganic nanoparticles including those made of gold. Gold nanoparticles (AuNPs) are among the most applied nanocarriers in biomedical fields (Pietro, Strano et al. 2016) thanks to the interesting elemental properties of gold, such as biocompatibility and chemical inertia. Although AuNPs are used for the conjugation of several molecules, there is a limited number of

studies on the effects of the conjugation of an AMP to them (Rai, Pinto et al. 2016).

2. Aims of the work

To optimize the biological properties of AMPs for their development as a new therapeutics, three different biochemical approaches were used.

- Design and synthesis of an analog of Esc(1-21) carrying three Aib residues at sequence position 1, 10 and 18 (Huang, Huang et al. 2010) to increase the α-helicity of the peptide and to enlarge its spectrum of activity. When inserted into the primary structure of peptides, Aib residues are expected to increase the α-helical content of the molecules, due to their strong helicogenicity. Importantly, a stabilized α-helical structure is known to be a crucial parameter for the AMPs' activity against Gram-positive bacteria (Giangaspero, Sandri et al. 2001) but also to increase their toxicity against mammalian cells (Huang, Huang et al. 2010). The Aib-containing peptide has been characterized for its structural and biological properties and compared with the parent peptide Esc(1-21).

- Design and synthesis of a diastereomer of Esc(1-21), named Esc(1-21)-1c, by replacing two L-amino acids in the C-terminal portion, i.e. L-Leu14 and L-Ser17, with the corresponding D-enantiomers. Besides making a peptide more resistant to enzymatic digestion, the insertion of D-amino acids is expected to disrupt the peptide's α-helical content (Hong, Oh et al. 1999) and to reduce its cytotoxicity. The effect(s) of D-amino acids incorporation on the structural/biological properties of the peptide have been investigated.

- Design and production of two different types of nano-systems to protect the AMP from proteolytic degradation and to allow its delivery to the target site without altering the antimicrobial properties: (i) inorganic gold nanoparticles (AuNPs) coated with Esc(1-21) and (ii) nano-embedded microparticles for pulmonary delivery of a model cationic AMP, i.e. colistin.

3. Results

3.1 – THE ANALOG OF Esc(1-21): [Aib$^{1, 10, 18}$]-Esc(1-21)

3.1.1 - Synthesis of [Aib$^{1, 10, 18}$]-Esc(1-21)

An analog of Esc(1-21) containing Aib residues was designed on the basis of the following considerations:

- The Aib residue in position 1 might prevent enzymatic degradation by aminopeptidases. It is known that an amidated C-terminus confers protection against carboxypeptidases (Rink, Arkema-Meter et al. 2010); therefore, the presence of an Aib residue at the C-terminus of Esc(1-21) would not be necessary. In comparison, the introduction of Aib residues along the primary structure is expected to be potentially beneficial for protection against endopeptidases.
- The α-helix-promoting capabilities of Aib are more effective when it is placed *internal* to the peptide sequence where it can display its influence on preceding and following residues in the peptide sequence.
- In [Fig. 12], the helical wheel plot of the primary structure of Esc(1-21) and its analog are shown, where the residues are arranged according to an ideal α-helical folding. In this conformation, it is possible to identify two faces, one hydrophobic and the other one with a more hydrophilic character. It is well known that in naturally-occurring Aib-rich peptides of fungal origin, named peptaibiotics, Aib residues are located within the hydrophobic face, but also at its boundary with the hydrophilic one (Toniolo, Peggion et al. 1994), (De Zotti, Biondi et al. 2012).

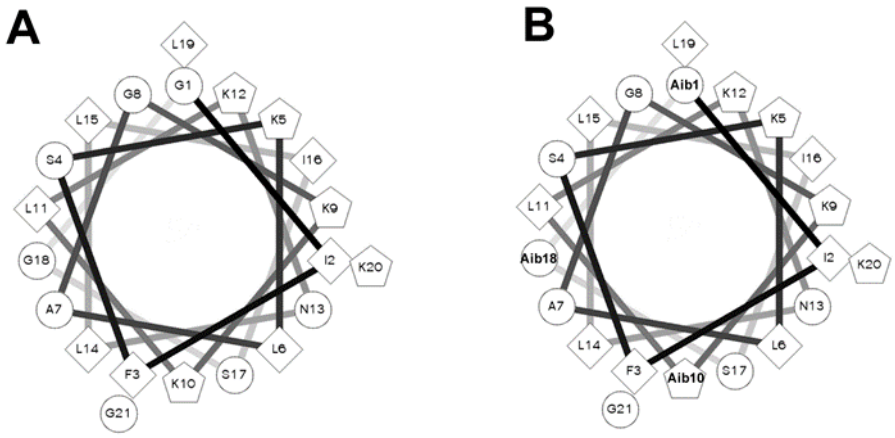

*Figure 12 - Helical wheel plots of the primary structure of Esc(1-21) (**A**) and [Aib[1,10,18]]-Esc(1-21) (**B**).*

Following these observations, three Aib residues were placed in the Esc(1-21) sequence: two of them as a replacement for the Gly 1 and Gly18, and the third one at the boundary between the hydrophobic/hydrophilic faces in substitution for Lys 10 [Tab. 4].

Table 4 – Comparison between the primary structure of Esc(1-21) and Aib[1,10,18]-analog. Aib residues are marked in bold.

Peptide	Sequence
Esc(1-21)	H-Gly-Ile-Phe-Ser-Lys-Leu-Ala-Gly-Lys-Lys-Ile-Lys-Asn-Leu-Leu-Ile-Ser-Gly-Leu-Lys-Gly-NH_2
[Aib[1, 10, 18]]-Esc(1-21)	H-**Aib**-Ile-Phe-Ser-Lys-Leu-Ala-Gly-Lys-**Aib**-Ile-Lys-Asn-Leu-Leu-Ile-Ser-**Aib**-Leu-Lys-Gly-NH_2

3.1.2 - Circular Dichroism

Far-UV Circular Dichroism (CD) spectra of Esc(1-21) and [Aib[1, 10, 18]]-Esc(1-21) were acquired in collaboration with Dr. Crisma and Dr. Biondi (Institute of Biomolecular Chemistry, Padova Unit, CNR). Three different solvents were used: water, trifluoroethanol (TFE) and 100 mM sodium-dodecyl sulfate (SDS) aqueous solution. In both membrane-mimicking environments, e.g. SDS and TFE, the spectra showed two negative maxima near 205 nm and 222 nm and a positive maximum at 195 nm [for the figures, please refer to those present in the work attached at the end of the manuscript: Biondi B., Casciaro B., di Grazia A., Cappiello F., Luca V., Crisma M. and Mangoni ML. "Effects of Aib residues insertion on the structural-functional properties of the frog skin derived peptide esculentin-1a(1-21)-NH_2". Amino Acids (2016) Oct 11]. This suggested a right-handed helical conformation for both peptides. Furthermore, the ellipticity ratio $R=[\theta]_{222}/[\theta]_{205}$ calculated in these environments highlighted a predominant α-helical conformation for both AMPs (Manning and Woody 1991). Differently, in water they adopted a random coil structure.

However, in TFE/water mixtures of varying composition (20%, 50% and 100%), the CD spectra of both peptides showed a significant difference. As indicated in Fig. 13, the set of spectra is characterized by an isodichroic point at 203 nm, which consists in two-state transition from the disordered conformation in water to the α-helical structure in 100% TFE. The helical content of the parent peptide increased with increased TFE concentrations (from 20% to 50% and much less from 50% to 100%), whereas the Aib^{1,10,18}-analog resulted to be more helical already at 20% TFE and the CD spectra slightly changed at higher TFE concentrations [Fig. 13].

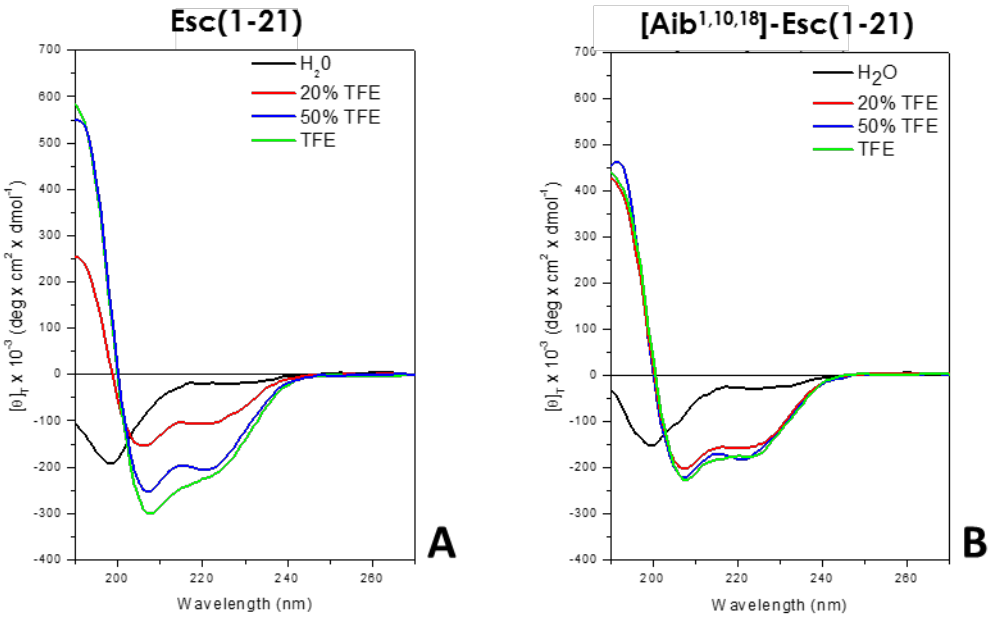

*Figure 13 - Far-UV CD spectra of Esc(1–21) (**A**) and [Aib^{1,10,18}]-Esc(1–21) (**B**) in water (black line), 20 % TFE (red line), 50 % TFE (blue line), and 100 % TFE (green line).*

3.1.3 - Antimicrobial activity

The antimicrobial activity of [Aib^{1,10,18}]-Esc(1-21) was tested by the microdilution broth assay to determine the MIC against Gram-negative, Gram-positive bacteria and yeasts. As shown in tab. 5, the MIC values of Esc(1-21) and its analog did not show any significant difference against Gram-negative bacteria and yeasts. In fact, Esc(1-21) and the analog had the same MICs against almost all the strains, with the exception of *Escherichia coli* ATCC 25922 and *Candida albicans* ATCC 10231 towards which the [Aib$^{1, 10, 18}$]-Esc(1-21) showed a 2-fold lower MIC than Esc(1-21).

Differently, [Aib$^{1, 10, 18}$]-Esc(1-21) resulted to be significantly stronger against Gram-positive bacteria with respect to the parent peptide. As shown in tab. 5, the MICs against *Staphylococcus epidermidis* strains were 8-fold lower than those of Esc(1-21), while the MICs against *S. capitis* 1 and *S. faecalis* ATCC 29212 were 16-fold lower. Furthermore, a 32-fold lower MIC was displayed by [Aib^{1,10,18}]-Esc(1-21) against *S. aureus* strain.

Therefore, the Aib residues replacement was found to be sufficient to confer Esc(1-21) a higher activity against Gram-positive bacteria without affecting its potency against Gram-negative bacterial strains and yeasts.

Table 5 - Antimicrobial activity of Esc(1-21) and [Aib^{1,10,18}]-Esc(1-21)

	MIC (μM)[a]	
Microorganisms	**Esc(1-21)**	**[Aib^{1,10,18}]-Esc(1-21)**
Gram-negative bacteria		
Acinetobacter baumannii ATCC 19606	2	2
Escherichia coli ATCC 25922	4	2
Escherichia coli D21	2	2
Pseudomonas aeruginosa ATCC 27853	4	4
Pseudomonas aeruginosa ATCC 19660	8	8
Yersinia pseudotuberculosis YPIII	1	1
Gram-positive bacteria		
Bacillus megaterium Bm11	2	0.5
Enterococcus faecalis ATCC 29212	>64	8
Staphylococcus aureus 6938	64	2
Staphylococcus capitis 1	64	4
Staphylococcus epidermidis ATCC 12228	16	2
Staphylococcus epidermidis 21	16	2
Staphylococcus hominis 1	1	1
Yeasts		
Candida albicans ATCC 10231	4	2
Candida guillier mondii	1	1

[a] *Values are those obtained from at least three readings out of four independent measurements*

3.1.4 - Cytotoxicity on mammalian cells

The cytotoxicity of Esc(1-21) and its analog was evaluated by the 3(4,5-dimethylthiazol-2yl)2,5-diphenyltetrazolium bromide (MTT) assay on two different types of mammalian cell lines: the human keratinocytes (HaCaT) cells and the human alveolar lung epithelial (A549 cells) after 24 h treatment.

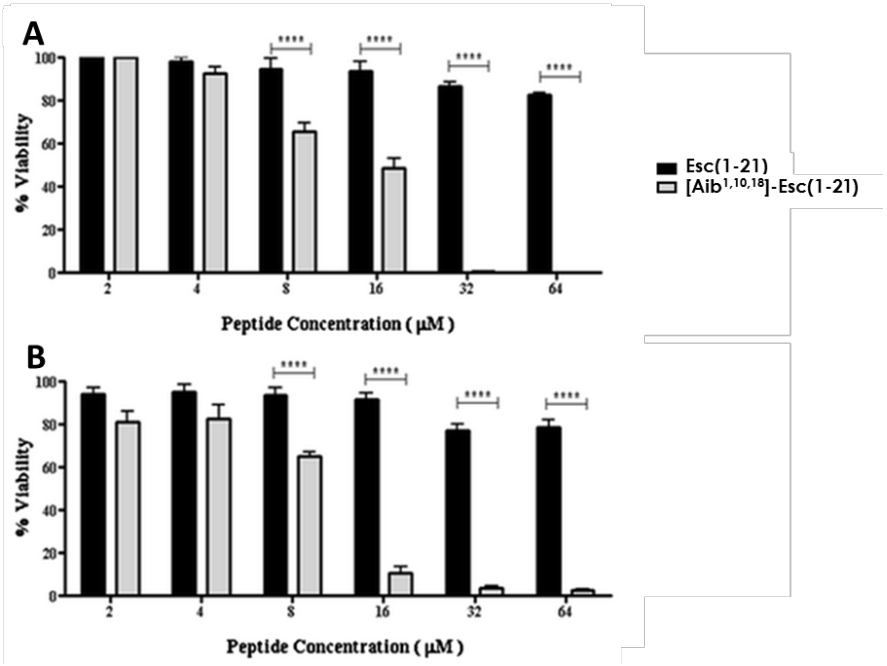

*Figure 14 - Peptides' effect on the viability of A549 cells (**A**) or HaCaT cells(**B**). About 4x10^4 cells were plated in each well of a microtiter plate in culture medium. After overnight incubation, the medium was replaced with 100 μl fresh medium supplemented with the peptides at different concentrations. After 24 h of peptide treatment, cell viability was determined by the MTT reduction to insoluble formazan. Cell viability is expressed as percentage with respect to the control (cells not treated with the peptide). Data points represent the mean of triplicate samples ± SEM. The levels of statistical significance between the two peptides are: ***p < 0.001; ****p < 0.0001*

As reported in Fig. 14, no significant differences were found when the two peptides were assayed against both cell lines at low concentrations (i.e. 2 and 4 μM).

Nevertheless, when the analogue was tested at higher concentrations, i.e. 32 and 64 μM, cell viability sharply decreased. This is in line with the higher content of α-helicity in the Aib-containing peptide, which is known to be critical for mammalian cell lysis (Gazit, Lee et al. 1994).

3.2 – THE ANALOG OF Esc(1-21): Esc(1-21)-1c

3.2.1 - Synthesis of Esc(1-21)-1c

With the aim to protect Esc(1-21) from proteolytic degradation and to reduce its toxicity against mammalian cells, an analogue named Esc(1-21)-1c was designed by replacing two L-amino acids with the corresponding D-amino acid enantiomers (L-Leu^{14} →D-Leu^{14}; L-Ser^{17}→D-Ser^{17}) [Tab. 6].

Table 6 - Primary structure of Esc(1-21) and Esc(1-21)-1c. D-amino acids are in italics.

Peptide	Sequence
Esc(1-21)	Gly-Ile-Phe-Ser-Lys-Leu-Ala-Gly-Lys-Lys-Ile-Lys-Asn-Leu-Leu-Ile-Ser-Gly-Leu-Lys-Gly-NH_2
Esc(1-21)-1c	Gly-Ile-Phe-Ser-Lys-Leu-Ala-Gly-Lys-Lys-Ile-Lys-Asn-***Leu***-Leu-Ile-***Ser***-Gly-Leu-Lys-Gly-NH_2

The diastereomer Esc(1-21)-1c was rationally designed on the bases of the following considerations:

- Several studies indicated that the reduction of α-helical content of a peptide correlated with its reduced ability in perturbing mammalian membranes causing cell lysis (Shai and Oren 1996), (Strahilevitz, Mor et al. 1994).
- D-amino acids are known to be α-helix breakers (Grieco, Carotenuto et al. 2013). Previous work performed with the shorter analog of Esc(1-21), [Esc(1-18)], indicated that the C-terminal half of this latter adopted an α-helical conformation in a hydrophobic environment mimicking the electrically neutral membranes of mammalian cells. Note that Esc(1-18)

differs from Esc(1-21) by a single amino acid in position 11 and lacks the C-terminal three residues tail. Since this tail contains two achiral glycine residues at positions 18 and 21, it is very unlikely that this region of Esc(1-21) folds in a stable helical conformation. On the contrary, replacement of two L-amino acids at positions 14 and 17 with the corresponding D-enantiomers would break the first turn of the α-helix expected to be present in the C-terminal half of Esc(1-21).

3.2.2 – Peptide stability in human serum

Biostability of both peptides was examined in the presence of 10% or 30% fresh human serum after 5 h and 24 h incubation at 37 °C in collaboration with Prof. Pini (Department of Medical Biotechnology, University of Siena). The data showed that the diastereomer Esc(1-21)-1c was more stable than the all-L Esc(1-21). As determined by HPLC (Tab. 7, refer to Fig. 15), the amount of non-degraded peptide was ~46% and 25% after 24 h incubation with 10% or 30% serum, respectively. The corresponding amount of Esc(1-21) was only ~22% and 11.5% [Tab. 7].

Table 7 - Peptide amount (%) after 5 h and 24 h incubation with human fresh serum at 37 °C

	Peptide amount (%)[a]			
	5 h		**24 h**	
Peptide	10% serum	30% serum	10% serum	30% serum
Esc(1-21)	44.4	20.95	22.19	11.5
Esc(1-21)-1c	63.34	30.12	45.61	25.46

[a]Peptide amounts were determined by the peak areas of the RP-HPLC relative to those of the control peptides (dissolved in PBS) at 0 min (set as 100 %) as demonstrated in Fig. 15.

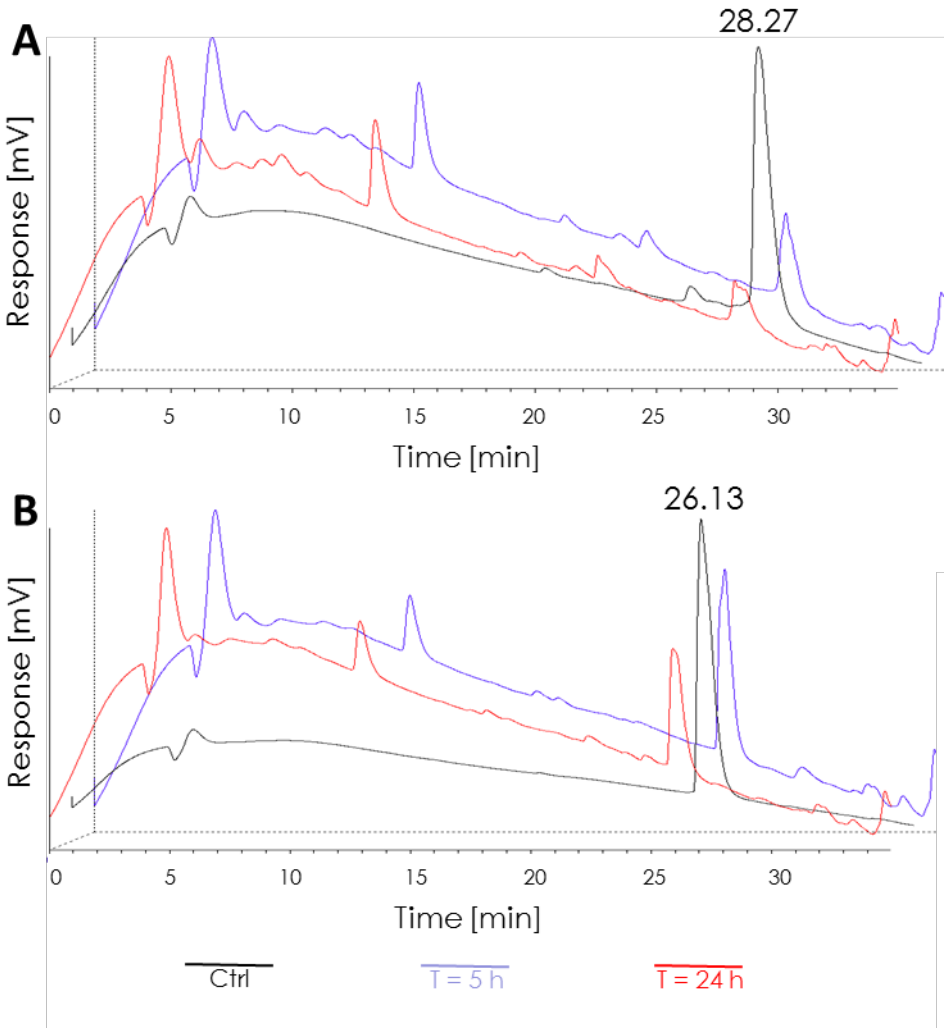

*Figure 15 - RP-HPLC profile of Esc(1-21) (**A**) and Esc(1-21)-1c (**B**) after 5 h [violet line] and 24 h [red line] incubation with 30% fresh human serum at 37 °C. The black line indicates the crude peptide dissolved in PBS (control, Ctrl). Percentages of peptide amount are also indicated. As explained in the legend to Table 7, they were determined by the peak areas at 28 or 26 minutes compared to the corresponding control peptide (Ctrl)*

3.2.3 - Structural properties

The secondary structure of both peptides was characterized by CD spectroscopy in the lab of Prof. Bhunia (Department of Biophysics, Bose Institute, India). The conformations adopted by Esc(1-21) and Esc(1-21)-1c were determined in: aqueous solution, SDS (a surfactant that mimics the anionic nature of bacterial membrane) and dodecylphosphocholine, DPC, (to mimic the zwitterionic nature of mammalian plasma membranes) [Fig. 16].

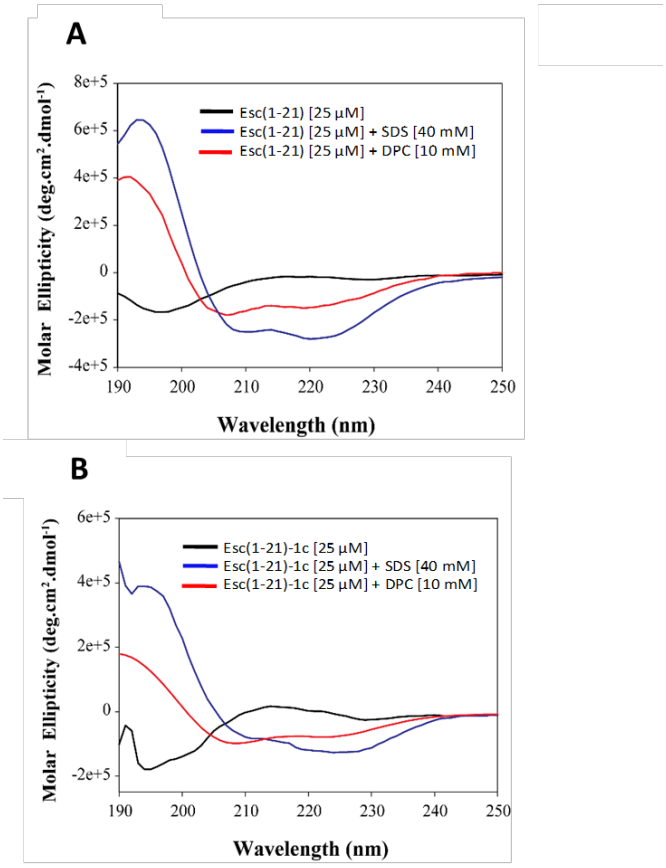

*Figure 16 - CD spectra of Esc(1–21) (**A**) and Esc(1–21)-1c (**B**) in aqueous solution [black line], 40 mM SDS [blue line] and 10 mM DPC [red line].*

In aqueous solution, the two peptides assumed a random-coil conformation. Differently, in DPC or SDS, both isomers adopted an α-helix conformation with higher helical propensity for Esc(1-21) compared to the diastereomer. The percentages of α-helix of the peptides in the three different environments are reported in [Tab. 8].

Table 8 - Percentage of α-helix content in the secondary structure of Esc(1-21) and Esc(1-21)-1c in aqueous solution, SDS and DPC.

	Helix content (%)	
Environment	**Esc(1-21)**	**Esc(1-21)-1c**
Aqueous solution	6	4
SDS	47	24
DPC	26	12

As expected, these results indicated a remarkable loss of α-helicity in the diastereomer, due to the incorporation of D-amino acids that break the α-helical structure. This effect was more pronounced in DPC and was also confirmed by NMR studies (performed in the laboratory of Prof. Bhunia). They revealed a flexible C-terminal arm in Esc(1-21)-1c compared to the all-L peptide [Fig. 17].

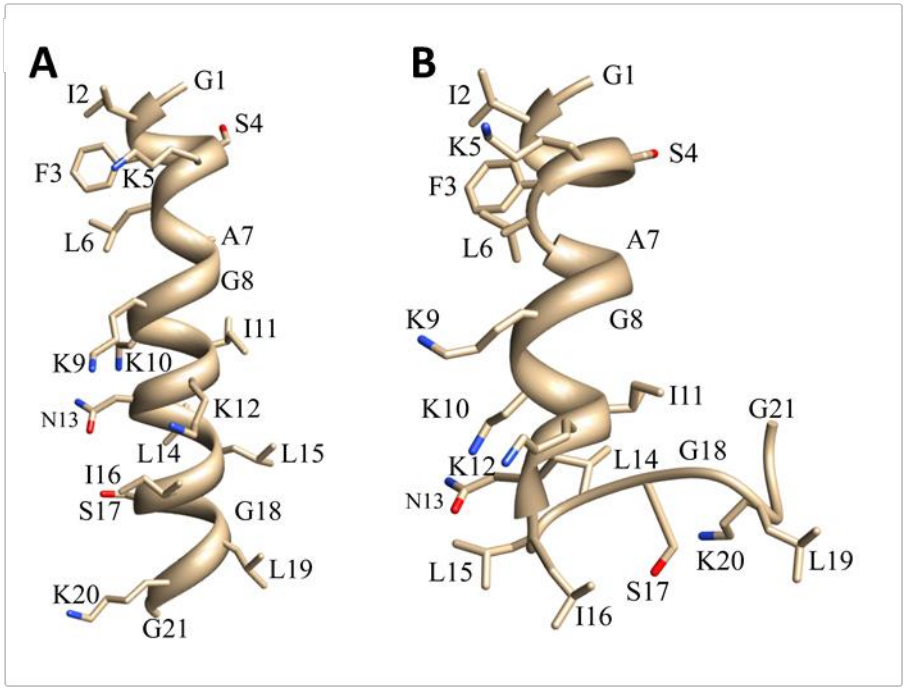

*Figure 17 - Three dimensional solution structures of Esc(1-21) (**A**) and Esc(1-21) (**B**) in DPC micelles. The cartoons represent the side chain orientation of a representative NMR structure of both peptides bound to DPC. These images were produced using the PyMOL software.*

3.2.4 - Antibacterial activity

The antimicrobial activity of Esc(1-21) and its diastereomer was tested against several strains of *P. aeruginosa* (either reference or clinical isolates from CF patients) in phosphate buffered saline (PBS). As shown in fig. 18, Esc (1-21) was able to cause about 99.9 % of *P. aeruginosa* strains within 30 min at a concentration of 1 μM. A weaker bactericidal activity was observed for the diastereomer Esc (1-21)-1c, being necessary a peptide concentration 4-fold higher

in order to achieve the same effect as that induced by the all-L parent peptide. However, at the same concentration used for the Esc(1-21) (1 μM) the diastereomer was capable of exerting a pronounced microbicidal activity causing approximately 90% killing of the bacterial population (dotted line in Fig. 18).

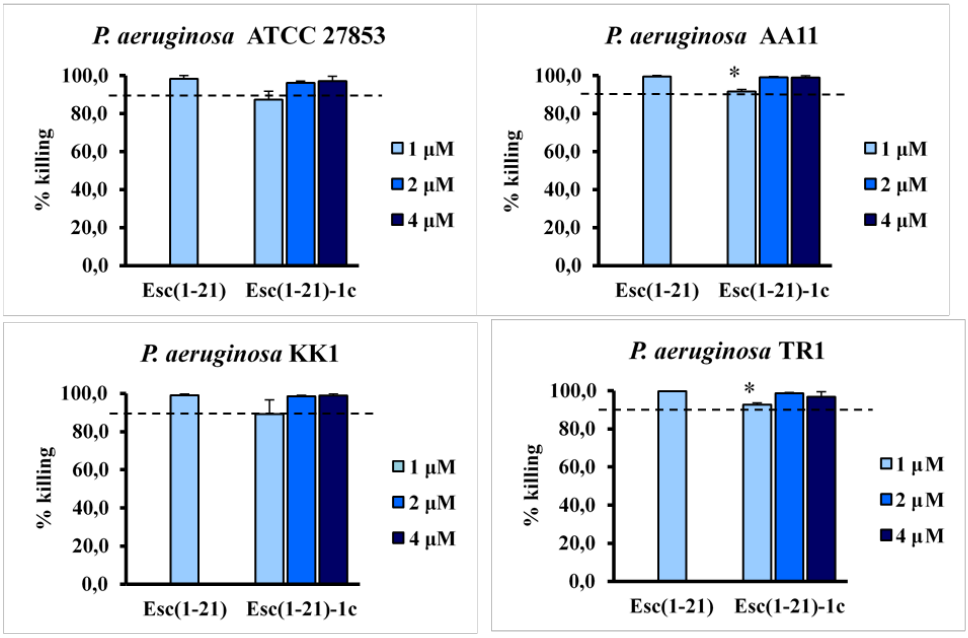

*Figure 18 – Antibacterial activity of Esc(1-21) and Esc(1-21)-1c against some P. aeruginosa strains after 30 min treatment. The results are the average of three different experiments ± SEM. Broken line represents 90% of killing. The levels of statistical significance between the two peptides are: *p < 0.05 (Student test).*

Remarkably, when the two peptides were tested against the sessile form of these strains, the diastereomer had a higher anti-biofilm activity than the all-L peptide on the clinical isolates AA11 and TR1, causing 95% killing of viable biofilm cells

at 12.5 μM compared to 25 μM of Esc(1-21) [please refer to the work attached at the end of the manuscript: "D-Amino acids incorporation in the frog skin-derived peptide esculentin-1a(1-21)NH_2 is beneficial for its multiple functions." By Di Grazia A, Cappiello F, Cohen H, Casciaro B, Luca V, Pini A, Di YP, Shai Y, Mangoni ML].

3.2.5 - Mode of action

3.2.5.1 - *Membrane perturbation assay on bacterial cells*

In order to investigate whether the diastereomer had a membrane perturbing activity on *Pseudomonas* cells, as already demonstrated for Esc(1-21) (Luca, Stringaro et al. 2013), the release of large intracellular compounds, such as the cytoplasmic β-galactosidase, from peptide-treated cells, was assessed. For this purpose, a recombinant *P. aeruginosa* strain constitutively expressing this enzyme was used (see Materials and Methods). Esc(1-21) provoked ~58 and 66% enzyme leakage at those concentrations (10 and 20 μM) causing the complete microbial death. A slight weaker damage was found for the diastereomer, as demonstrated by the minor leakage of β-galactosidase (~ 49 and 62 % at 10 and 20 μM, respectively) at the same peptide concentrations causing ~100% microbial killing.

3.2.5.2 - *Membrane perturbation assay on lipid vesicles*

To investigate whether the membrane perturbing activity of the peptides was not a stereospecific mechanism mediated by recognition of chiral targets, e.g. proteins, carboxyfluorescein (CF)-loaded liposomes were used. The membrane permeability can be tested by entrapping a fluorescent molecule, i.e. CF, in the water volume inside the lipid vesicles at high concentration. This induces self-association and quenching of the dye (Stella, Mazzuca et al. 2004). After peptide addition, the membrane perturbation leads to probe release and dissociation with a resulting fluorescence increase.

Both peptides were tested at different concentrations on PE/PG liposomes (7:3 *v:v*, 200 μM), which mimic the lipid composition of the anionic membrane of Gram-negative bacteria. As shown in Fig. 19, Esc(1-21) showed a stronger membrane perturbing activity compared to the diastereomer, as indicated by the higher fluorescence values obtained 30 min after peptide addition to the lipid vesicles.

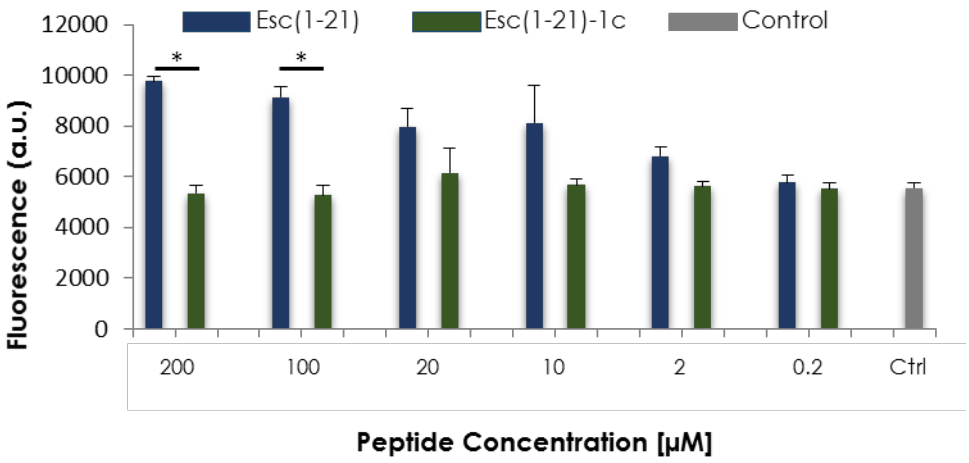

*Figure 19 - Fluorescence intensity after 30 min from the addition of both peptides to PE/PG liposomes (7:3, v:v). Control (Ctrl) is given by lipid vesicles not treated with the peptide. Data points represent the mean of triplicate samples ± SD. The levels of statistical significance between the two peptides are: *p < 0.05*

This is in agreement with the results of the β-galactosidase assay and the higher activity of Esc(1-21) against the free-living form of *P. aeruginosa* compared to the diastereomer. In addition, it can be excluded that a stereospecific interaction with a membrane receptor is involved in the mechanism of membrane perturbation of both peptides.

3.2.6 - Cytotoxicity on mammalian cell lines

The effect of the two peptides on the viability of two different cell lines was analyzed by the MTT assay. In particular, the cytotoxic effect of both Esc(1-21) and Esc(1-21)-1c was tested on A549 cells and mammalian macrophages Raw

264.7 after 24 h treatment with different peptide concentrations. Esc(1-21)-1c resulted to be less toxic than the parent peptide at the highest concentrations used against both types of cells. This is presumably due to its lower α-helical content compared to Esc(1-21). [For the figures, please refer to those present in the work attached at the end of the manuscript: "D-Amino acids incorporation in the frog skin-derived peptide esculentin-1a(1-21)NH_2 is beneficial for its multiple functions." By Di Grazia A, Cappiello F, Cohen H, Casciaro B, Luca V, Pini A, Di YP, Shai Y, Mangoni ML].

3.3 – PEPTIDE CONJUGATION TO NANOPARTICLES: AuNPs@Esc(1-21)

3.3.1 - Synthesis of AuNPs@Esc(1-21)

AuNPs were synthetized by citrate reduction of gold and found to have an average size of ~ 14 nm [Fig. 20].

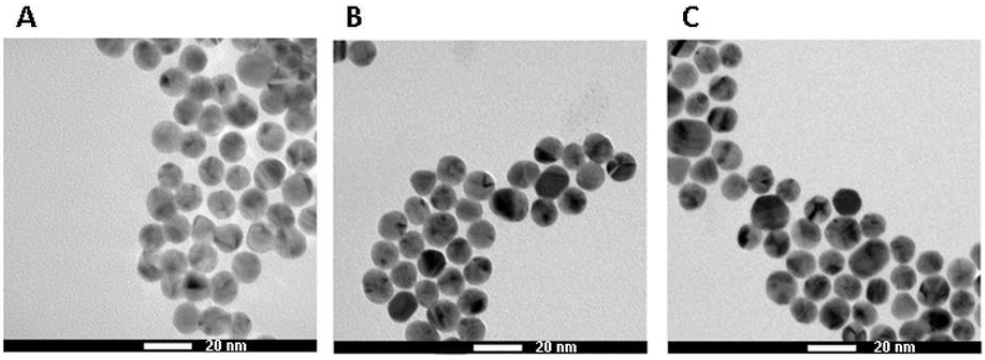

*Figure 20 – Transmission electron microscopy (TEM) analysis of AuNPs. A small volume of AuNPs was dropped onto a TEM grid and after drying, was imaged using a TEM Tecnai F20. AuNPs as synthesized (**A**). AuNPs@PEG (**B**). AuNPs@Esc(1-21) (**C**). Scale bar: 20 nm.*

As shown in fig. 20, AuNPs preserved the same size and spherical shape in every step of their synthesis. With the aim to increase their stability, a bifunctional poly(ethylene glycol) (PEG) bearing a thiol and a carboxylic group was used [SH-EG(8)-$(CH_2)_2$-COOH]. The two reactive groups are important for the functionalization of AuNPs: the PEG was attached to the AuNPs *via* a gold-thiol

bond (AuNPs@PEG); while the carboxylic group was used for further derivatization with the peptide *via* carbodiimide-mediated coupling.

The carboxylic groups of the AuNPs@PEG were activated with different amounts and ratios of 1-ethyl-3-(3-dimethylaminopropyl)-carbodiimide) (EDC) and N-hydroxysulfosuccinimide (Sulfo-NHS) and the stability of the nanoparticles was assessed by UV-Vis spectroscopy, measuring the absorbance of the maximum peak at 519 nm and the absorbance at 600 nm (Ivanov, Bednar et al. 2009). For stable AuNPs, the ratio between absorbance value at 519 and 600 nm should be higher than 4, while for aggregated NPs the ratio decreases. As the NPs stability depends on a delicate balance between charges, with the aim to optimize the covalent linkage of the peptide, four different conditions were assayed [Tab. 9]. The addition of three different ratios and amounts of EDC:sulfo-NHS led to a slight aggregation of the AuNPs@PEG, as shown by the UV-Vis spectra and the resulting absorbance ratio [Fig 21A,B,C]. In comparison, as indicated in [Fig. 21D], the activation with 2.5 μmol of EDC and 4.6 μmol of sulfo-NHS maintained the stability of AuNPs@PEG. For this reason, this ratio was selected for the addition of the peptide.

Table 9 - Amounts of EDC and sulfo-NHS used for activation of AuNPs@PEG and corresponding stability condition (i.e. aggregation or non-aggregation)

Condition	EDC (µmol)	Sulfo-NHS (µmol)	Aggregation?
1	10	18.4	Yes
2	2,5	9,2	Yes
3	5	8,4	Yes
4	2.5	4,6	No

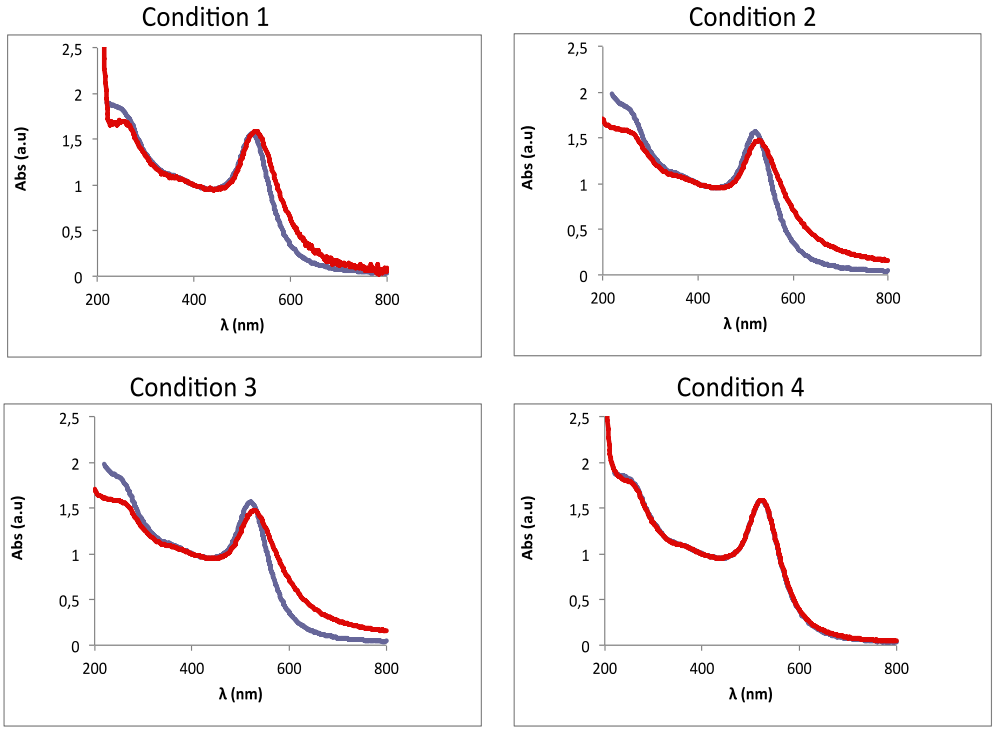

Figure 21 - UV−Vis spectroscopy of the AuNPs@PEG without EDC and sulfo_NHS (blue line) and the same NPs activated using the conditions indicated in table 11 (red line). To assess the stability of the AuNPs@PEG, the ratio 519/600 nm was calculated. Only using condition number 4 the AuNPs@PEG remained stable.

After activation, different amounts of Esc(1-21) ranging from 1.5 µg to 4 µg were added to the same quantity of AuNPs@PEG. As shown by UV-spectra, the addition of 3 µg [Fig. 22C] and 4 µg [Fig. 22D] led to aggregated nanoparticles (absorbance ratio 519/600 nm lower than 4). The addition of 1.5 µg and 2 µg [Fig 22A, B] maintained AuNPs@PEG stability. Therefore, 2 µg of Esc(1-21) were used as an optimal amount for the functionalization without causing precipitation of the negatively-charged AuNPs@PEG during the coupling process.

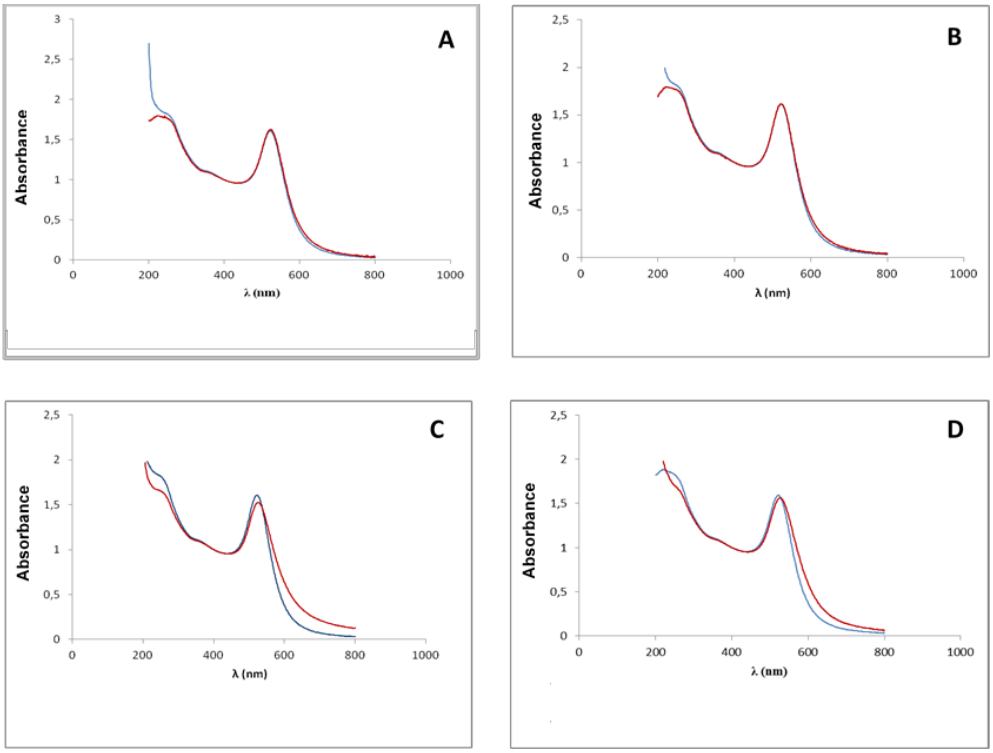

*Figure 22 - UV−Vis spectroscopy of the AuNPs@PEG (blue line) obtained from condition 4 (Tab. 11) compared to AuNPs@Esc(1-21) (red line) obtained after conjugation of AuNPs@PEG with a different amount of peptide: 1.5 µg (**A**); 2 µg (**B**); 3 µg (**C**); 4 µg (**D**).*

As indicated in the experimental section, the amount of peptide in the supernatant (not attached to the AuNPs@PEG) was then quantified. By knowing the amount of peptide added to the sample for functionalization, it was possible to determine by difference the amount of peptide bound to the AuNPs@PEG: 0.7 μg of peptide resulted to be conjugated to 20 pmol of AuNPs@PEG, resulting in about 16 molecules of peptide per AuNP@PEG. The comparison between the molar concentration of AuNPs@Esc(1-21) and the corresponding molar concentration of peptide coated onto AuNPs@PEG is shown in [Tab. 10].

Table 10 - Comparison between molar concentration of AuNPs@Esc(1-21) and the corresponding molar concentration of Esc(1-21).

Molar concentration of AuNPs@Esc(1-21)	**Molar concentration of peptide coated onto AuNPs@Esc(1-21)**
20 nM	0.35 μM
10 nM	0.17 μM
5 nM	0.08 μM

3.3.2 - Antipseudomonal activity

The free Esc(1-21) was tested against a high bacterial cell density i.e. 4 x 10^8 CFU/mL (which was needed to prepare samples for the electron microscopy) and found to provoke 50% killing of the planktonic form of *P. aeruginosa* within 20 minutes at 1 μM (MBC_{50}, minimal bactericidal concentration causing at least 50% of bacterial death). However, when the peptide was coated onto AuNPs@PEG, it was more active with a MBC_{50} ~ 12 fold lower than that of the free form (0.08 μM, Tab. 11). Interestingly, AuNPs@Esc(1-21) were found to have a significantly

higher activity also against the biofilm form of *P. aeruginosa* with a minimal bactericidal concentration causing at least 50% of eradication of biofilm ($MBEC_{50,}$) ~ 17 fold lower than that of the free peptide within 2 h of treatment. Importantly, no lethal activity was displayed by AuNPs@PEG against both forms of *P. aeruginosa.*

Table 11 - Antimicrobial activity of Esc(1-21) and AuNPs@Esc(1-21) on both free living and biofilm forms of P. aeruginosa ATCC 27853

	Antibacterial Activity	
	Planktonic form	**Biofilm form**
Compound	**MBC_{50}**	**$MBEC_{50}$**
Esc(1-21)	1 μM	3 μM
AuNPs@Esc(1-21)	5 nM (=0.08 μM peptide)	10 nM (=0.17 μM peptide)

3.3.3 - Mechanism of antipseudomonal activity

To investigate whether the conjugation to AuNPs affected the membrane-perturbing activity of Esc(1-21), the Sytox Green assay was performed [Fig. 23]. Sytox Green is a membrane-impermeable probe whose fluorescence intensity enhances upon binding to DNA, once it has entered cells with a perturbed cytoplasmic membrane. When AuNPs@Esc(1-21) were used at 10 nM, a concentration causing approximately 70% bacterial death of the planktonic form (data not shown), a fast increase of fluorescence intensity was noted after their addition to the bacteria. This suggests that a higher membrane damage was induced by AuNPs@Esc(1-21) with respect to the same amount of free peptide.

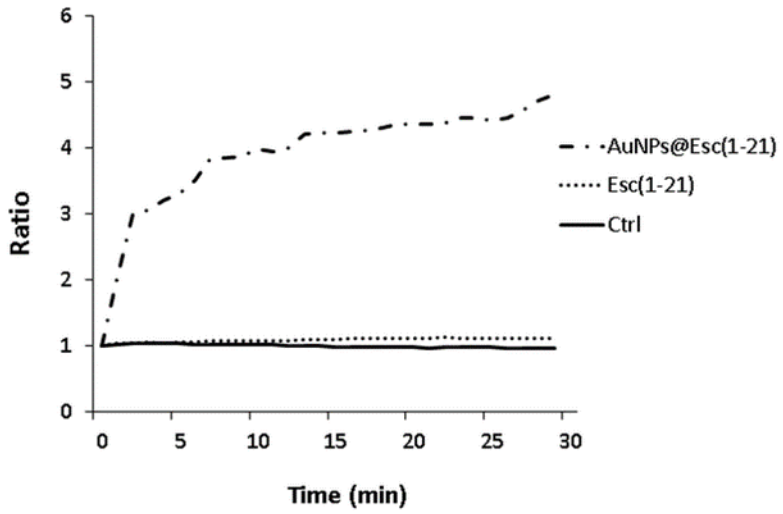

Figure 23 - Kinetics of cytoplasmic membrane permeabilization of P. aeruginosa ATCC 27853 (4 x 10^8 CFU/ml) induced by 10 nM AuNPs@Esc(1-21) or the corresponding concentration of free Esc(1-21). Once basal fluorescence reached a constant value, 10 nM AuNPs@Esc(1-21) or AuNPs@PEG as well as the equivalent concentration of free Esc(1-21) were added, and changes in fluorescence (λ_{exc}= 485 nm, λ_{ems} = 535 nm) were monitored for 30 min. Control (Ctrl) was given by buffer-treated bacteria. The ratio of each value to the initial one measured after 1 min from NPs/peptide addition is reported on the y-axis. The values represent the mean of triplicate samples from a single experiment, representative of three different experiments.

The effect of the membrane-perturbing activity of AuNPs@Esc(1-21) at their MBC_{50} was also visualized by electron microscopy. The planktonic form of *P. aeruginosa* ATCC 27853 was treated with AuNPs@Esc(1-21) and AuNPs@PEG at different incubation times. As visualized by scanning electron microscopy (SEM) [Fig. 24], AuNPs@Esc(1-21) appeared to be located on the microbial surface already after 1 min incubation with bacteria compared to the control sample and to the AuNPs@PEG-treated bacteria. After 8 min treatment, AuNPs@Esc(1-21) formed clusters around the cells at various points and caused membrane disruptions, with leakage of intracellular material [Fig. 24, arrows].

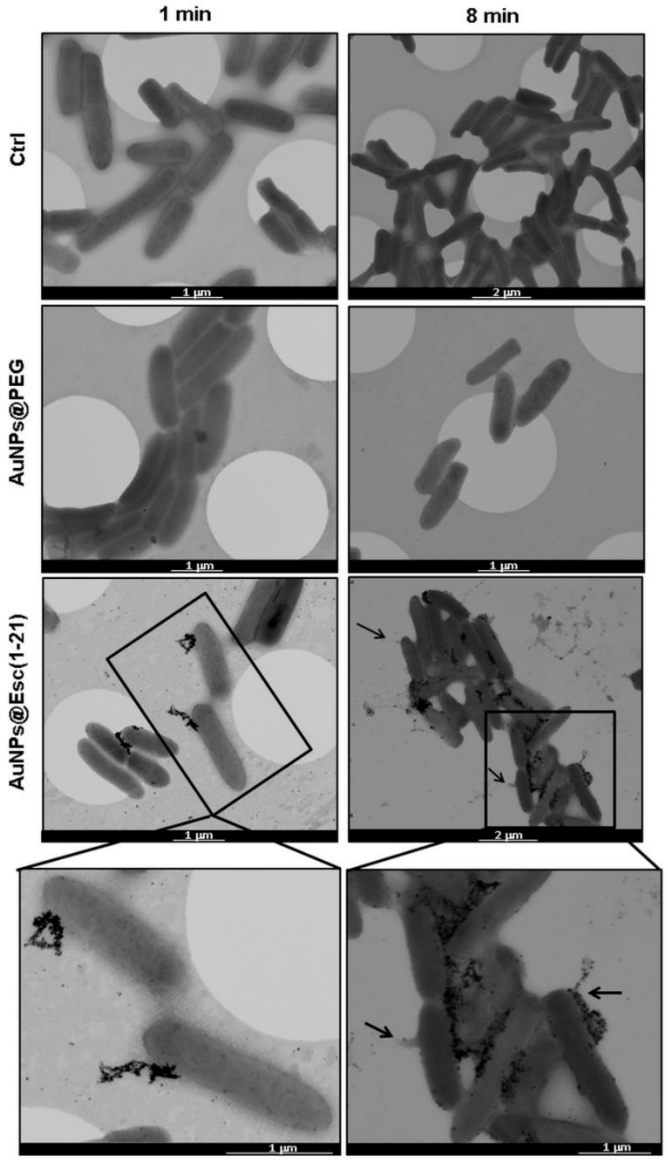

Figure 24 - SEM images of P. aeruginosa ATCC 27853 cells after 1 min (left panels) or 8 min (right panels) treatment with AuNPs@Esc(1-21) at the MBC_{50} or with AuNPs@PEG, at the same molar concentration. Controls (Ctrl) were buffer-treated cells. Insets are magnifications of image areas indicated by the black frame. Arrows indicate cell debris.

This outcome became more pronounced after 15 min treatment with a drastic change in the bacterial shape and a marked disintegration of the cellular structure, as shown by TEM [Fig. 25].

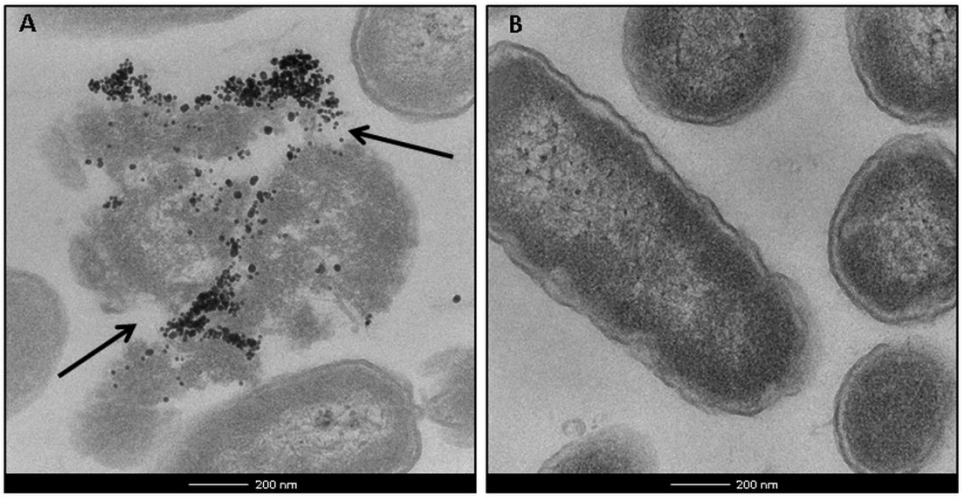

*Figure 25 - TEM micrographs of P. aeruginosa cells after 15 min treatment with AuNPs@Esc(1-21) at the MBC_{50} (**A**) or buffer (**B**). Black arrows indicate lysed bacterial cells. Scale bar: 200 nm*

A schematic representation of AuNPs@Esc(1-21) and their effect on P. *aeruginosa* is reported in [Fig. 26].

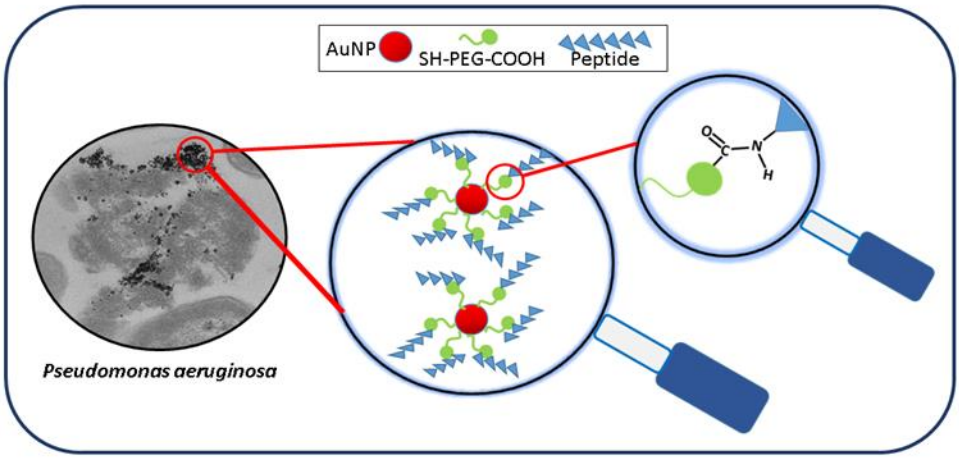

Figure 26 - Schematic representation of the synthesized AuNPs@Esc(1-21) and their damage caused on P. aeruginosa cells.

3.3.4 - Antipseudomonal activity after pre-treatment with a proteolytic enzyme

AuNPs@Esc(1-21) were found to retain their antipseudomonal activity after pre-treatment with a proteolytic enzyme, e.g. trypsin. In fact, when both the free peptide and the conjugated AuNPs@Esc(1-21) (at their MBC_{50}) were pre-treated with trypsin, only ~ 13% of bacterial killing was obtained for the free peptide (about 4-fold reduction of activity). On the contrary, no significant change in killing activity was manifested by AuNPs@Esc(1-21) after incubation with trypsin [Fig. 27]. This is likely due to the higher resistance of Esc(1-21) to proteolytic degradation upon its coating to AuNPs@PEG.

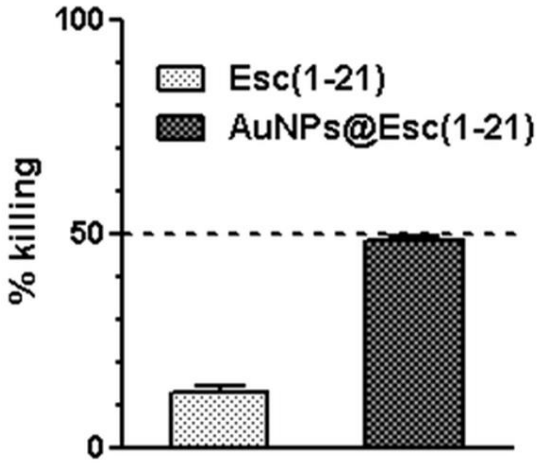

Figure 27 - Antipseudomonal activity of Esc(1-21) or AuNPs@Esc(1-21) at their MBC50 (1 μM and 5 nM, respectively) after treatment with trypsin (0.02 μg/mL). The percentage of bacterial killing was calculated compared to the control (buffer-treated bacterial cells) and is reported on the y-axis. Dotted line indicates 50% bacterial killing. Data points are the mean of triplicate samples ± SEM of three independent experiments.

3.3.5 – Cytotoxicity on human keratinocytes

Both AuNPs@Esc(1-21) and AuNPs@PEG were tested for their cytotoxicity on human cells, i.e. keratinocytes (HaCaT cells) by the MTT assay. According to published papers showing harmless effects of AuNPs (Chatterjee, Bandyopadhyay et al. 2011) or Esc(1-21) (Di Grazia, Cappiello et al. 2015), both NPs showed negligible toxicity. In particular, both peptide-coated and non-coated NPs were unable to reduce the number of metabolically active cells within 2 h [Fig. 28] and 24 h treatment up to the highest concentration used (e.g. 60 nM, which corresponds to 12 x MBC_{50}).

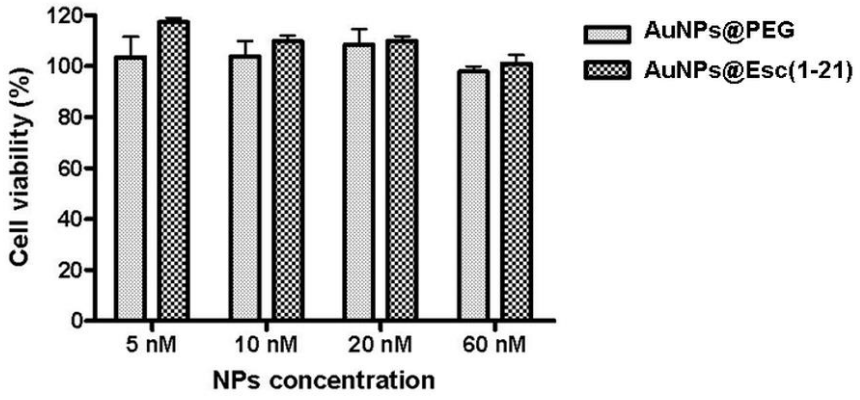

Figure 28 - Effects of AuNPs@PEG or AuNPs@Esc(1-21) on the viability of HaCaT cells after 2 h treatment. Cell viability was determined by the MTT reduction to insoluble formazan. The percentage represents the cell viability with respect to the control. Data points are the mean of triplicate samples ± SEM of three independent experiments.

3.3.6 - Pseudo-wound healing activity on a keratinocytes monolayer

As reported in the literature (Di Grazia, Cappiello et al. 2015), Esc(1-21) has been found to have the capability to stimulate *in vitro* the migration of mammalian cells, e.g. keratinocytes and bronchial epithelial cells. To verify whether the conjugation to AuNPs affected the AMP's ability to promote migration of keratinocytes, a pseudo-wound healing assay was carried out by means of special cell culture inserts (see Materials and Methods). As shown in Fig. 29, AuNPs@Esc(1-21) were able to retain the ability of the peptide to induce re-epithelialization by migrating HaCaT cells. The functionalized NPs promoted the closure of the pseudo-wound in the HaCaT monolayer within 9 h and with a similar rate to that displayed by a 3-fold higher concentration of free Esc(1-21), i.e. 0.25 μM.

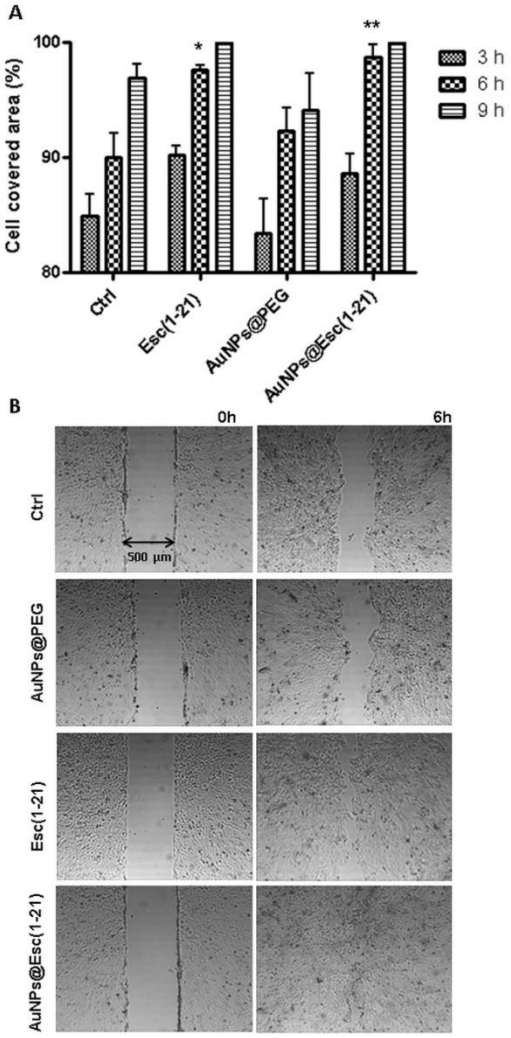

*Figure 29 - Effect of AuNPs@PEG, Esc(1-21) and AuNPs@Esc(1-21) on the closure of a pseudo-wound field produced in a monolayer of HaCaT cells, seeded in each side of an ibidi culture insert. (**A**): Cells were grown to confluence and afterwards, they were treated with 5 nM AuNPs@PEG, AuNPs@Esc(1-21) or with 0.25 µM Esc(1-21). Cells were photographed at the time of insert removal (0 h), examined for cell migration after 3, 6 and 9 h, and compared to the control (Ctrl.) All data are the mean of three independent experiments ± SEM. The levels of statistical significance between Ctrl and treated samples are indicated as follows *p < 0.05, **p < 0.01. (**B**): Micrographs showing representative results of pseudo-"wound" closure after 6 h treatment.*

3.4– ENGINEERED NANOPARTICLES FOR THE LOCAL DELIVERY OF A CATIONIC AMP

Another important strategy to allow AMPs to efficiently cross biological barriers (e.g. the lung mucus and the extracellular matrix of biofilm communities) before reaching the target infectious site and to prolong their therapeutic effect is given by the design of appropriate nano-embedded microparticles (NEM). Using colistin (Col, Fig. 30) as a model cationic AMP, inhalable dry powders consisting in biocompatible and biodegradable synthetic polymers (i.e. PLGA) loaded with colistin and included in micrometric inert carriers (e.g. lactose, mannitol), already employed in inhaled medicines, were developed. Col is the only AMP currently used for treatment of lung infections in CF patients (Uttley, Harnan et al. 2013). However, its poor lung bioavailability and elevated therapeutic dosage (160 mg twice a day delivered by nebulization of a Col solution) make it a drug of last resort for treatment of bacterial infections.

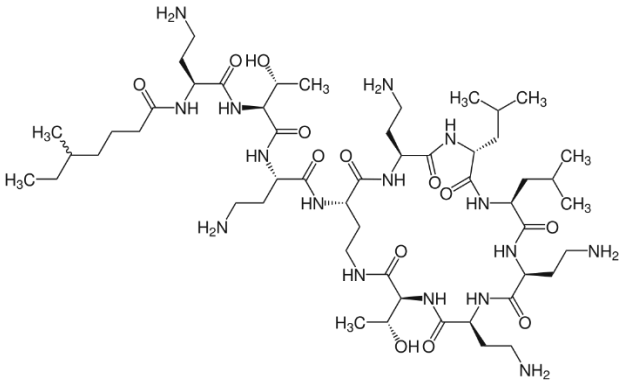

Figure 30 - Chemical structure of colistin

The aforementioned formulations should: (i) land in the lungs; (ii) deliver AMP-loaded NPs upon dissolution of the inert carrier; (iii) shield AMP interactions with mucus/biofilm promoting drug availability to bacteria; (iv) prolong drug release and allow the establishment of higher drug gradients in the mucus layer.

3.4.1 - Synthesis and Properties of colistin-loaded nanoparticles

Thanks to the expertise of Dr. d'Angelo (University "Federico II", Naples, Italy) Col-loaded nanoparticles (NPs) made of PLGA were produced by emulsion/solvent diffusion technique in the presence of chitosan (CS) or poly(vinyl alcohol) (PVA). Both CS-modified and PVA-modified NPs resulted to have a diameter of 300 nm; a spherical core-shell structure, as shown by TEM images [Fig. 31] and a similar Col entrapment efficiency (63 ± 1 % and 60 ± 2 % for Col-CS and Col-PVA NPs, respectively). Nevertheless, a difference on NPs zeta potential was observed (+12.4 ± 2.1 and -7.1 ± 1.4 for Col-CS and Col-PVA NPs, respectively), likely attributed to the presence of CS or PVA on particle surface.

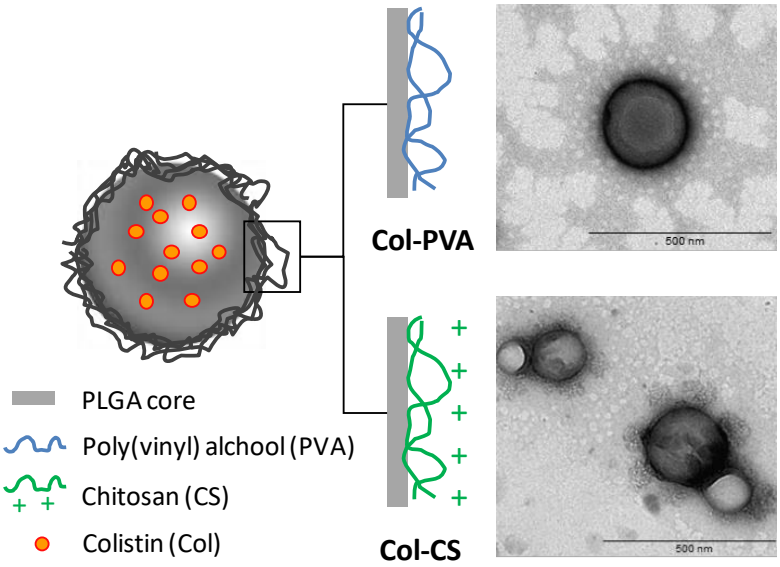

Figure 31 - Schematic representation of the Col-loaded PLGA-based NPs and the corresponding TEM images

The two formulations also were observed to have a different *in vitro* kinetic of Col-release. In Fig. 32 the percentages of Col released over time at physiological condition (pH 7.2 and 37° C) are reported: CS-NPs showed a more rapid kinetic in the first hours of incubation with respect to the PVA-modified NPs. Indeed, while 50% of Col was released within 6 hours from CS-NPs, no more than 5% was released from PVA-NPs. However, after an initial burst, both formulations sustained Col release for approximately 15 days.

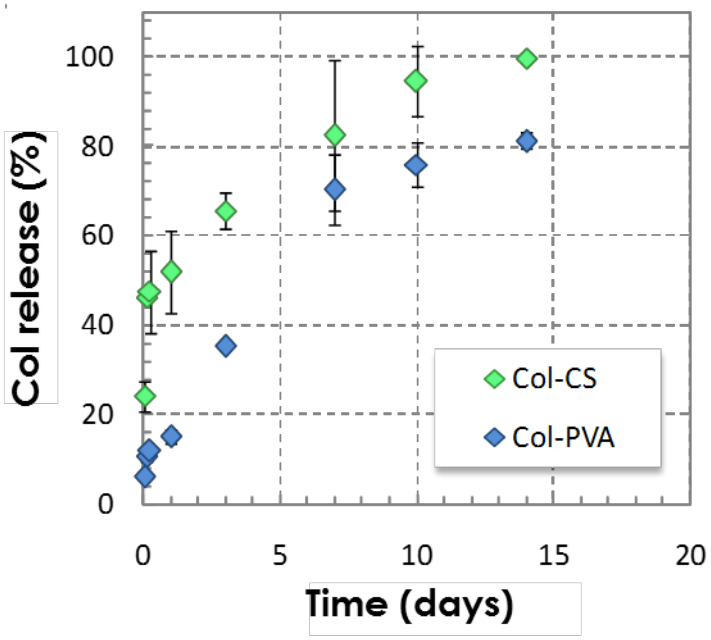

Figure 32 - Release profiles of Col in PBS at pH 7.2 and 37 °C for both formulations: Col-CS in green and Col-PVA in blue. Experiments were done in triplicate for each time point of release kinetics and the results are expressed as percentage of Col released from NPs ± SD over time (n = 6).

The interactions between NPs and mucin appears to be crucial for an efficient penetration across the pulmonary mucus layer. The transport of Col-loaded NPs through artificial CF mucus was determined using a Transwell-multiplate assay. The stronger interaction of CS-modified NPs, with respect to PVA-NPs, led to a faster diffusion of NPs across the artificial mucus layer. Indeed, as reported in [Fig. 33B] more than 70% of the initial CS-NPs passed through the mucus layer in the first 6 hours, while for PVA-NPs only 40% of the initial amount was found in the acceptor compartment of the transwell plate. When the free Col was tested in the same assay, it was not able to diffuse through the mucus up to 24 hours.

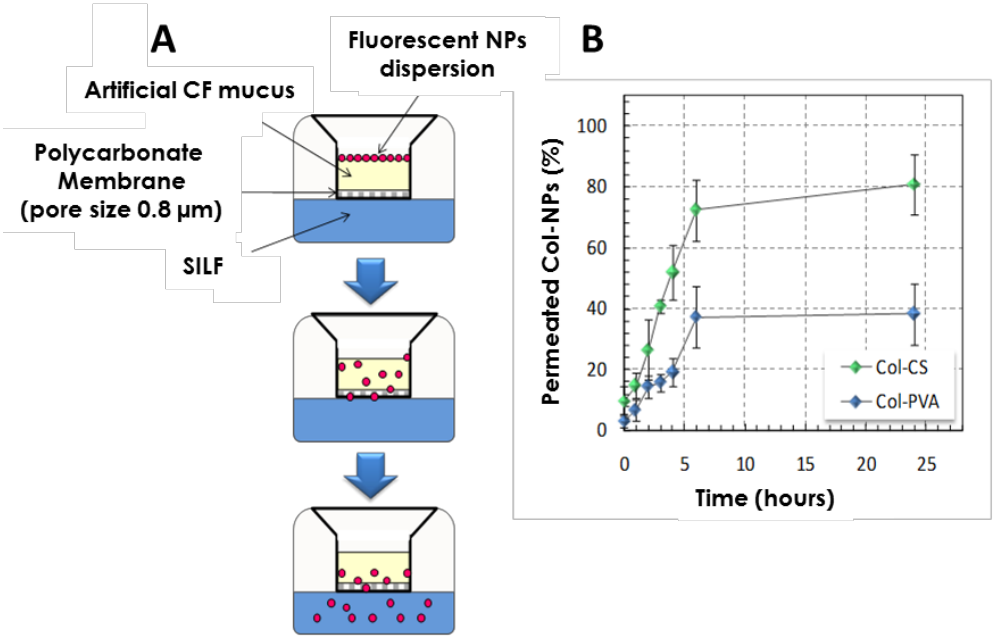

*Figure 33 - Transport of Col-loaded NPs through artificial CF mucus as determined by the Transwell multiplate assay. Schematic representation of the experimental set-up (A); percentage amount of Col-loaded NPs permeated across the artificial mucus layer as a function of time (**B**). Data are mean ± SD of values calculated on three different batches (*n = 6*).*

3.4.2 – Properties of colistin-loaded NEM

The surface-engineered NPs (CS and PVA-modified) were embedded into microparticles in order to produce NP-based dry powders for the delivery of Col in the respiratory tract and lung. The microparticles were produced using an inert carrier (*i.e.* lactose) through an optimized spray-drying process. As indicated by SEM analysis [Fig. 34], the obtained NEM (Col-CS_L and Col-PVA_L) resulted to be spherical with a geometric diameter ranging from 6.4 µm to 8.3 µm. The formulations were characterized for their *in vitro* aerosolization properties to evaluate if the spray-drying process with lactose could interfere with the NPs

properties: both size and ζ-potential of Col-CS and Col-PVA NPs remained unchanged after the process (data not shown).

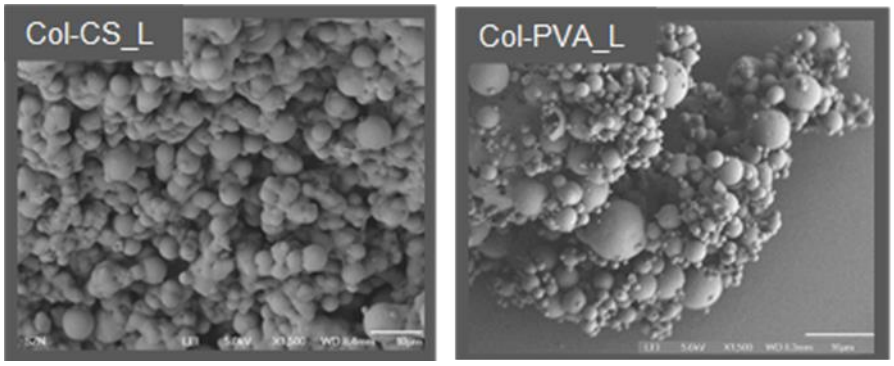

Figure 34 - SEM images of optimized lactose microparticles embedding engineered PLGA NPs: Col-CS_L NEM (*left*) and Col-PVA_L NEM (*right*)

3.4.3 - *In vitro* activity on *P. aeruginosa* biofilm

The antimicrobial activity against *P. aeruginosa* biofilm was tested on the reference strain of *P. aeruginosa* ATCC 27853. The ability of the free Col and the two NEM formulations to eradicate biofilm was evaluated at different incubation times (24, 48 and 72 h). As expected, the free Col was able to eradicate 90% of biofilm biomass within the first 24 h, but this effect was significantly diminished after 48 h and completely lost after 72 h. In comparison, the Col-loaded NEMs showed a different anti-biofilm activity: despite a weaker biomass reduction (~ 50%) was found during the first 24 h of treatment at 7.5 and 15 μg/ml, this activity was preserved for 72 h. More precisely, this effect was retained for 72 h by the Col-PVA, while the anti-biofilm activity of Col-CS NEMs resulted to be less pronounced at the last time point. This outcome may be due to the different kinetic of Col release from the two NEMs [Fig. 35].

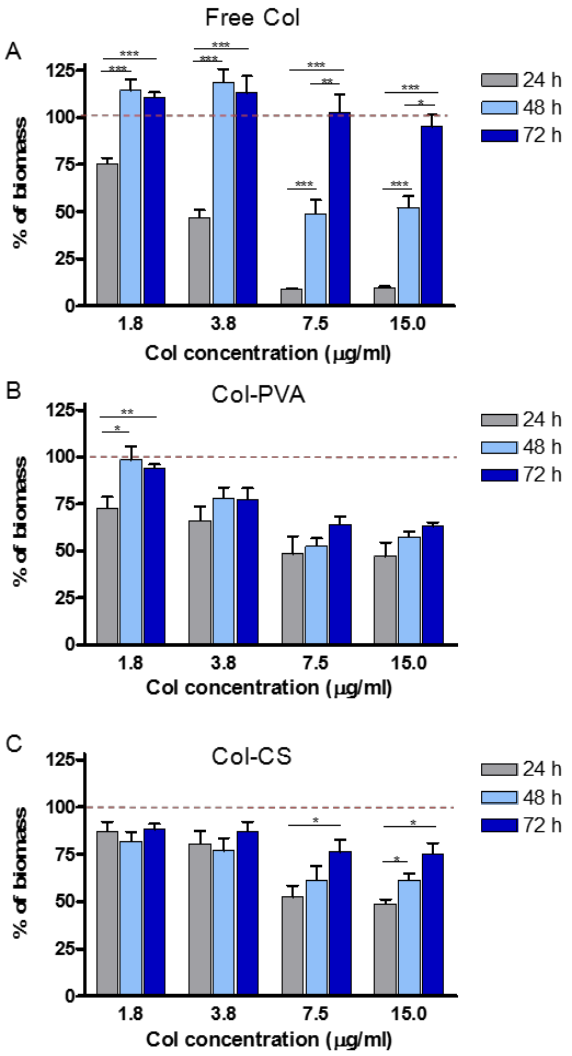

*Figure 35 - Percentage of P. aeruginosa ATCC 27853 biofilm biomass after 24 h, 48 h and 72 h treatment with free Col (A), Col-PVA_L NEM (**B**) and Col-CS_L NEM (**C**) compared to the control sample (100% biofilm biomass, red broken line). All data are the mean of at least three independent experiments ± SEM. The level of statistical significance between groups was calculated by the Student's* t *test and is indicated as follows: *,* $p < 0.05$*; ***$p < 0.01$*;***,* $p < 0.001$*.*

3.4.4 - Penetration of fluorescent NPs inside *P. aeruginosa* biofilm

Confocal microscopy analysis was performed to verify the ability of Col-loaded formulations to penetrate inside *P. aeruginosa* biofilm. In Fig. 36, *P. aeruginosa* ATCC 27853 biofilm treated for 24 h with NEM incorporating fluorescent NPs is shown. The red color indicates the distribution of rhodamine-labeled NPs while the green fluorescence shows the SYTO®-9-labeled biofilm bacteria. In particular, the higher green fluorescence intensity observed in some points may represent the intracellular DNA released by damaged cells and to which SYTO®-9 strongly binds.

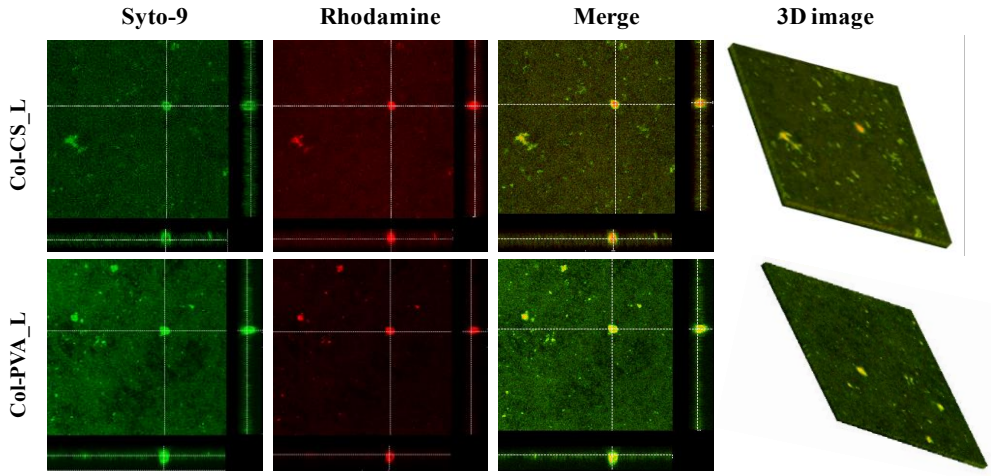

*Figure 36 - Confocal analysis of preformed P. aeruginosa ATCC 27853 biofilm after 24 h treatment with fluorescent Col-CS_L or Col-PVA_L NEM at 3.8 μg/ml Col concentration. Biofilm cells were stained and visualized using SYTO®-9, while rhodamine-labeled NPs were used to produce Col-loaded NEM. Each panel shows reconstructions from the top in the large panel and sides in the right and bottom panels (*xy, yz, *and* xz *dimensions). Three-dimensional reconstructions of biofilms are shown on the far right panel (3D image).*

4. Discussion

Microbial infections currently cause millions of deaths every year and the growing emergence of microorganisms resistant to the available drugs has become a worldwide problem for human health. With the onset of antibiotic resistant strains, new molecules able to eradicate bacterial infections are urgently needed. AMPs hold promise for the development of new anti-infective agents and the scientific research is focusing on their discovery and characterization. AMPs show different mechanisms of action, but most of them have a membrane-perturbing activity on microbial cells. This non-specific mode of action very rarely leads to microbial resistance, because the bacterium should completely change the composition of the cytoplasmic membrane; an event that would cause significant harm to the microorganism itself. However, bringing AMPs to the clinical development requires to overcome some of their limitations, e.g. low biostability, cytotoxicity and the difficulty in reaching the infection site at active concentrations. These disadvantages remain to be solved before a breakthrough in the search for new antibiotic compounds.

In the last years, a frog-skin derived AMP named Esc(1-21) was studied for its antimicrobial activity against a feared human pathogen, i.e. the Gram-negative bacterium *P. aeruginosa* (Luca, Stringaro et al. 2013). It was previously demonstrated by CD spectroscopy that Esc(1-21) adopted an α-helical conformation when tested in PE/PG liposomes (7:3 *w/w*) mimicking the anionic nature of the plasma membrane of Gram-negative bacteria. As demonstrated by *in vitro* assays, Esc(1-21) displayed a higher activity against Gram-negative bacteria compared to Gram-positive ones. This is presumably due to its own biophysical

properties. Structure-activity relationship studies have demonstrated that several parameters can influence the spectrum of action and the potency of α-helical AMPs, e.g. the amino acid sequence, the length, the net charge, the overall hydrophobicity, the amphipathicity, the α-helical content, and the oligomeric state. All of these parameters are strictly related and slightly modifications in one of them can result in significant changes in one or more of the others. Some studies have proved that peptide's helicity is an important factor for the perturbation of biological membranes and for the peptide's microbicidal activity against Gram-positive bacteria (Giangaspero, Sandri et al. 2001). For these reasons, an analog of Esc(1-21) bearing three strongly helicogenic Aib residues in its primary structure was designed and synthesized. In order to confer the peptide a higher resistance to proteases (e.g. aminopeptidases and endopeptidases) and a higher α-helical content, three Aib residues were used to replace the N-terminal amino acid ($Gly^1 \rightarrow Aib^1$) as well as the internal lysine 10 (i.e. $Lys^{10} \rightarrow Aib^{10}$) and Gly 18 ($Gly^{18} \rightarrow Aib^{18}$). From the data obtained by CD spectroscopy [Fig. 13], at increasing concentrations of TFE (from 20% to 50%), the Aib-analog appeared to be much more helical with respect to the parent peptide. Furthermore, the analog [$Aib^{1,10,18}$]-Esc(1-21) acquired a greater antibacterial activity against Gram-positive bacteria, while maintaining its efficacy against Gram-negative strains and yeasts. It is not easy to give a clear explanation to the different behavior of the two peptides against the three different classes of microorganisms. Differences in the phospholipid composition of the membrane of these microorganisms as well as in the organization of their cell wall could be the main reason accounting for the different activities. In fact, before reaching the target cytoplasmic membrane, AMPs need to interact with the lipopolysaccharides-outer

membrane in Gram-negative bacteria or with the peptidoglycan/glucan-rich layer in the cell wall of Gram-positive bacteria/yeasts, respectively. Probably, more stringent structural requirements of [Aib^{1,10,18}]-Esc(1-21) may favor its translocation through the peptidoglycan barrier into the plasma membrane of Gram-positive bacteria. This may in part justify its lower MIC values compared to those of the parent peptide (See Tab. 5).

Yet, a higher α-helicity resulted in increased cytotoxicity (at a peptide concentration range from 16 μM to 64 μM) against some eukaryotic cell lines (i.e. HaCaT and A549 cells). This is in agreement with previous studies showing that both α-helix conformation and its stability are crucial factors for mammalian membrane perturbation and cell lysis (Gazit, Lee et al. 1994), (Shai and Oren 1996). However, at the antimicrobial concentrations of 2 μM and 4 μM, [Aib^{1,10,18}]-Esc(1-21) turned out to be harmless as the parent peptide. Overall, on the basis of these results, it can be stated that the insertion of three Aib residues in Esc(1-21) leads to the production of an analog with a greater activity against Gram-positive bacteria without increasing its cytotoxicity at those concentrations inhibiting bacterial growth (see Tab. 5). Nevertheless, due to the toxicity of [Aib^{1,10,18}]-Esc(1-21) towards human cells at concentrations higher than the MICs, it would be better to develop this peptide not for clinical usage, but in the agriculture field for the formulation of biocides to prevent contamination of agriculture lands by both Gram-positive and Gram-negative bacteria.

Another approach used in this thesis to simultaneously decrease the susceptibility of Esc(1-21) to proteolytic enzymes and its cytotoxicity, was the incorporation of D-amino acids in the peptide sequence. This is because D-amino acids: (i) are

resistant to animal proteases (Weinstock, Francis et al. 2012) and (ii) are known to be "α-helix breakers" (Grieco, Carotenuto et al. 2013). More specifically, a diastereomer of Esc(1-21) containing D-Leu14 and D-Ser17 [Esc(1-21)-1c)] was designed and synthesized. The effects of these two L- to D-amino acids substitution in Esc(1-21) were studied on both structural and biological activities of the peptide and compared with those of the wild-type Esc(1-21). As demonstrated by CD analysis, both peptides adopted an α-helix conformation in anionic and zwitterionic environments, e.g. SDS and DPC, respectively. However, compared to Esc(1-21), the insertion of the two D-amino acids significantly reduced the α-helical content of the peptide in zwitterionic lipids mimicking the electrically-neutral membrane of mammalian cells. This can explain the significantly reduced cytotoxicity of the diastereomer to different types of human cells, compared to Esc(1-21) or to the more helical and more cytotoxic Aib-analog. Remarkably, this change in the secondary structure slightly affected the antibacterial activity of the peptide against the planktonic form of *P. aeruginosa*, which correlates to other examples in the literature (Oren and Shai 1997) . In addition, the diastereomer resulted to be (i) more effective against the sessile form of *P. aeruginosa*, which is much more difficult to eradicate and (ii) more stable in human serum. All together these results contribute to make Esc(1-21)-1c a more promising candidate for future pharmaceutical preparations against *Pseudomonas*-induced infections.

Amino acids replacement is not the only strategy to increase the stability of a peptide to proteolytic degradation. Moreover, this approach does not allow a peptide to overcome biological barriers (e.g. mucus, skin layers) before reaching

the site of infection at high active concentration. A different biochemical approach to this purpose is given by the use of nano-systems. It is increasingly evident from the literature that the use of nanoparticles has revolutionized the field of biomedicine (Cabuzu, Cirja et al. 2015). Among the various nanoparticles synthesized in recent years, gold nanoparticles (AuNPs) have attracted most attention due to their small size, high solubility and stability. Non-functionalized AuNPs have been shown to be biocompatible, chemically inert and biologically harmless because of the gold elemental properties (Connor, Mwamuka et al. 2005), (Williams, Ehrman et al. 2006). It is now known that the reported antibacterial activity of non-functionalized AuNPs can be attributable to chemical compounds formed during NPs synthesis and not completely removed from them (Zhang, Shareena Dasari et al. 2015). AuNPs are one of the most used NPs in diagnostic and biomedicine (Reznickova, Novotna et al. 2015), (Tsai, Lu et al. 2015).

However, the designed AuNPs@Esc(1-21) have represented an innovation: for the first time, it has been shown how a chemical conjugation of an AMP *via* a PEG linker to AuNPs (synthetized by the citrate reduction of gold), increases its antimicrobial activity while retaining its mode of action and harmless effect on human keratinocytes. As pointed out in tab. 11, AuNPs@Esc(1-21) were more efficient in killing both forms of *P. aeruginosa* compared to the activity explicated by the same concentration of the free peptide. This is indicated by the lower MBC_{50} and $MBEC_{50}$ values (see tab. 11) compared to those found for Esc(1-21) and this is likely due to the higher local concentration of peptide molecules at the site of bacterium-NPs contact.

Indeed, packaging peptide molecules within the same NP would enable not only to protect the peptide from proteolytic degradation, but also to enhance its local concentration reaching doses much higher than dose achievable after administration of free peptides. It is worthwhile noting that the conjugation of Esc(1-21) to AuNPs@PEG did not affect the bacterial membrane-perturbation of the peptide. An evidence to support this statement was provided by the results of the Sytox Green assay and the electron microscopy analysis, which showed the leakage of cytosolic compounds already after 8 min from peptide addition to the bacteria. In addition, the SEM/TEM images proved that the bare AuNPs@PEG were not detected on the bacterial cell surface. This highlights that Esc(1-21) is the driving force allowing AuNPs@Esc(1-21) to reach the bacterial membrane and to perturb it.

Furthermore, the conjugation of the peptide to AuNPs@PEG did not result in higher cytotoxicity and was found to preserve the peptide's capability to stimulate cell migration in a pseudo-"wound" healing assay on a keratinocytes monolayer. This suggests their ability to accelerate recovery of a wound in a skin layer, following bacterial infection. Importantly, it was recently demonstrated that AuNPs can pass through different types of animal tissues and through the stratum corneum barrier, depending on their size, shape and charge (Greish, Thiagarajan et al. 2012). All these results and considerations make AuNPs@Esc(1-21) attractive nano-formulation for the topical treatment of skin infections.

Remarkably, *P. aeruginosa* not only colonizes ulcers and skin wounds but also the mucus in the lungs of cystic fibrosis (CF) patients, leading to serious chronic infections that classical antibiotics can hardly reach and eradicate. It is therefore

necessary a pharmaceutical formulation able to reach the site of infection and to provide a prolonged drug release, avoiding multiple drug administrations.

Many studies have been conducted in recent years to characterize PLGA NPs for pulmonary drug release. Their small size makes them suitable molecules to overcome the airway barrier and to target specific lung cells. A previous study demonstrated that modulation of NPs' size and surface with PVA and CS can be of great help to facilitate their transport through the mucus (Ungaro, d'Angelo et al. 2012).

As for the AuNPs@Esc(1-21), the CS/PVA-PLGA NPs were designed to (i) protect the peptide from proteolytic degradation; (ii) let it reach the site of infection at high concentrations and to (iii) provide a sustained peptide release in order to prolong the peptide's therapeutic effect. In this case, however, CS and PVA-PLGA NPs were loaded with a model AMP (i.e. Col) currently employed for treatment of *P. aeruginosa* lung infections in CF patients. Both formulations were embedded into an inert carrier forming inhalable dry powders (Nano-embedded microparticles, NEM).

The two engineered-NPs showed a high percentage of entrapment efficiency (≥ 60% of Col) but a difference in drug release. PVA-modified NPs provided a slow and sustained Col release lasting for 15 days; in comparison, CS-modified NPs showed an initial higher "burst" followed by a slower release kinetics (see Fig. 31). Furthermore, the Col-CS NPs diffused more easily through an artificial CF mucus than Col-PVA NPs, whereas the free Col did not succeed in penetrating it. This in an important outcome for the future treatment of *Pseudomonas*-induced infection in CF patients: indeed, the resistance of the biofilm form of *Pseudomonas* to the currently used antibiotics is mainly due to their inability to

penetrate the mucus made of alginates and other extracellular polysaccharides. Interestingly, it was demonstrated that both NEMs formulation were able to penetrate the bacterial biofilm and to release Col overtime (72 h). Moreover, both CS and PVA modified NPs were found to enhance the activity of Col against *P. aeruginosa* biofilm at long-term (up to 72 h), while the free peptide was no longer effective beyond 24 h. The gradual release of Col from NEMs, especially from the PVA-NPs, allowed a prolonged exposure of the drug to the biofilm communities, with a resulting higher efficiency in biofilm eradication at long-time.

Taken all together, these results suggest that engineered microembeeded PLGA NPs represent a fascinating technical approach to encapsulate novel antimicrobials such as Esc(1-21) for treatment of *P. aeruginosa* lung infection. Future studies will focus on the design and manufacturing of these type of formulations, likely containing Esc(1-21) for the development of new antipseudomonal strategies.

5. Conclusions and future perspectives

Presently, AMPs represent one of the most promising future strategies for the development of new antimicrobial compounds to eradicate bacterial infections, most of which have become resistant to the available antibiotics.

In spite of their great potential as templates for the manufacturing of new drugs, only a small number of AMPs has entered into clinical trials. This is mainly due to some disadvantages including low peptide bioavailability, high toxicity, and high susceptibility to proteolytic degradation. On the basis of the structure-activity relationship (SAR) studies on thousands of AMPs, it has been possible to know the main physicochemical parameters playing a crucial role in their mechanism of action.

Furthermore, the rapid progress in the field of nanotechnology has suggested the usage of peptide-coated nanoparticles as valuable carriers not only to prolong the peptide's half-life but also to overcome biological barriers (e.g. lung mucus, biofilm extracellular matrix) that a peptide needs to face before reaching its target site.

On the basis of this knowledge, either substitution of natural amino acids with non-coded residues or peptides conjugation to inorganic/polymeric NPs have been used in this work to rationally optimize the antimicrobial properties of cationic peptides, e.g. the frog-skin derived AMP Esc(1-21) and the currently used colistin.

Importantly our results have indicated that these approaches represent encouraging methodologies to improve the antimicrobial properties of AMPs and for the

generation of new peptide-based formulation for an efficient treatment of different types of infectious diseases.

Taken all together, these results encourage us to continue to investigate the interesting biological properties of Esc(1-21) analogs, e.g. Esc(1-21)-1c, to better understand the biochemical parameters responsible for their antimicrobial features. In addition, these peptides could be used for the development of novel gold and polymeric nanoparticles-based therapeutic formulation.

6. Materials and Methods

6.1 – MATERIALS

Chemically synthesized Esc(1-21) and the diastereomer Esc(1-21)-1c were purchased from Selleck Chemicals (Houston, TX, USA). [Aib^{1,10,18}]-Esc(1-21) was synthesized by the group of Dr. Marco Crisma, University of Padova. Dulbecco's modified Eagle's medium (DMEM), heat-inactivated fetal bovine serum (FBS), non–essential amino acids (NEAA), sodium pyruvate (100 mM), penicillin/streptomycin, glutamine and gentamycin were from Euroclone (Milan, Italy). Sytox Green was obtained from Molecular Probes (Leiden, The Netherlands); 3(4,5-dimethylthiazol-2yl)2,5-diphenyltetrazolium bromide (MTT), Hank's buffer, colistin sodium sulphate (Col), polyvinyl alcohol (PVA), Triton-X 100 and trypsin from bovine pancreas were from Sigma-Aldrich (St. Louis, MO). Ultrapure chitosan (CS) was obtained from NovaMatrix (Oslo, Norway). All other chemicals were reagent grade.

6.2 – MICROORGANISMS

The microorganisms used for the antimicrobial assays were:

- **Gram-negative** bacteria: the reference *Pseudomonas aeruginosa* ATCC 27853 and the clinical isolates *P. aeruginosa* AA11, KK1 and TR1. In addition, the reference *Acinetobacter baumannii* ATCC 19606, *Escherichia coli* D21, *E. coli* ATCC 25922 and *Yersinia pseudotuberculosis* YPIII were used. Furthermore, the *P. aeruginosa* PAO1 strain carrying plasmid pPrsal190 (Rampioni, Schuster et al. 2007), (Rampioni, Polticelli et al. 2007), kindly provided by Prof. Livia Leoni

(Roma Tre University, Rome, Italy), was used for the β-galactosidase activity assays.

- **Gram-positive** bacteria: the reference *Staphylococcus epidermidis* ATCC 12228 and *Bacillus megaterium* Bm11 as well as the clinical isolates *S. aureus* 6938, *S. capitis* 1, *S. epidermidis* 21 and *S. hominis* 1.
- **Yeasts:** the reference *Candida albicans* ATCC 10231 and *C. guiller mondii* from the frog natural flora (Mangoni, Miele et al. 2001).

6.3 – CELL CULTURES

The human type II alveolar epithelial cell line A549 (from the American Type Culture Collection, Manassas, Va), the human immortalized keratinocytes (HaCaT) cell line and the murine Raw 264.7 macrophage cell line were employed. Macrophages and A549 cells were cultured in DMEM supplemented with 10% FBS, 2 mM L-glutamine and antibiotics (0.1 mg/mL of penicillin and streptomycin) at 37 °C and 5 % CO_2 in 25-cm^2 flasks. In the case of macrophages, NEAA and sodium pyruvate were also added. For HaCaT cells, 4 mM L-glutamine and 0.05 mg/mL of gentamicin were added to the medium.

6.4 – METHODS

6.4.1 – Circular dichroism (CD) spectroscopy

CD spectra of Esc(1-21) and [$Aib^{1,10,18}$]-Esc(1-21) were measured on a Jasco (Hachioji City, Japan) model J-715 spectropolarimeter equipped with a Haake thermostat, while CD spectra of Esc(1-21) and Esc(1-21)-1c

were measured on a Jasco 815. A fused quartz cell of 0.1 mm path length (Hellma, Mühlheim, Germany) was used. Measurements were collected at 25 °C and at 0.1 nm wavelength intervals in the 190- 300 nm range.

6.4.2 – Liposomes preparation

Peptide-membrane interaction can be investigated by the use of liposomes as model membranes, due to their bilayer structure, which is in principle identical to the lipid organization of biological membranes (Mouritsen 2011). Liposomes were prepared by dissolving the lipids in a 2:1 (*v/v*) chloroform/methanol solution, i.e. phosphatidylethanolamine/ phosphatidylglycerol (PE/PG) at a ratio 7:3 (*v/v*). The solvents were then evaporated under reduced argon atmosphere until a thin film was formed. The lipid film was hydrated with CF solution [Fig. 37] in 10 mM phosphate buffer containing 140 mM NaCl and 0.1 mM EDTA, pH 7.4. CF was entrapped inside liposomes at a self-quenching concentration, i.e. 30 mM. The liposome suspension was subjected to 10 freeze and thaw cycles and extruded through two stacked polycarbonate membranes with 100 nm pores to obtain unilamellar vesicles. The final lipid concentration was determined by the Stewart phospholipids assay (Stewart 1980).

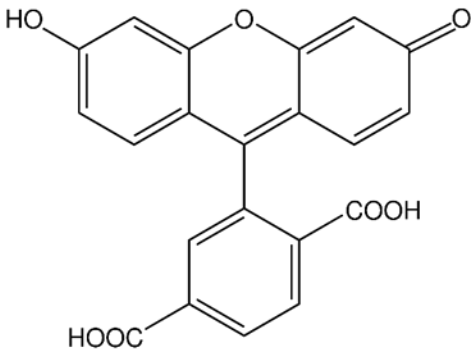

Figure 37 - Chemical structure of carboxyfluorescein

The obtained liposomes were separated from the free dye by gel filtration on a 40 cm Sephadex G-50 column.

6.4.3 – AuNPs: synthesis and characterization

AuNPs were synthesized by the citrate reduction method as previously described (J. Turkevitch, P.C. Stevenson, et al 1951), (G. Frens 1973). Hydrogen tetrachloroaureate (III) (0.235 mmol) was dissolved in 200 mL of Milli-Q water and magnetically stirred under reflux. Sodium citrate dehydrate was then added [Fig. 38]. The solution was kept under ebullition and protected from light for 30 min.

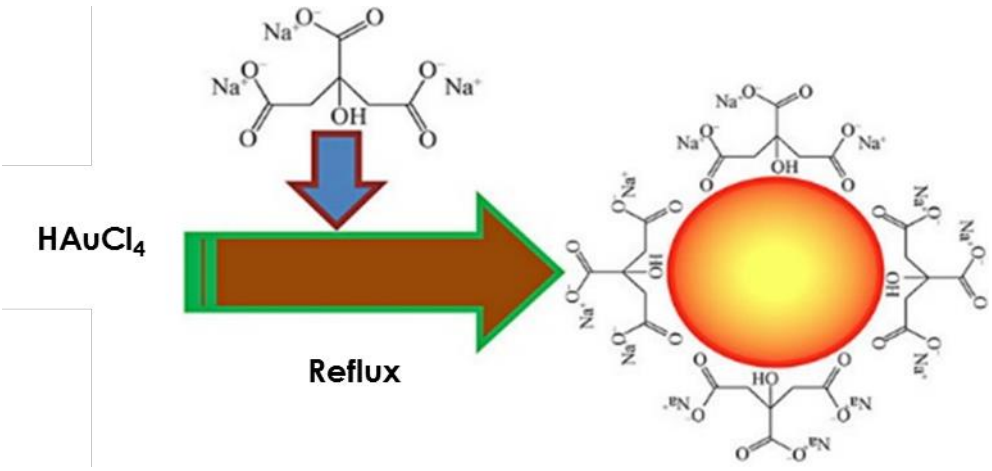

Figure 38 - Schematic representation of the synthesis of AuNPs

The obtained AuNPs were characterized by ultraviolet-visible (UV-vis) spectroscopy (Cary 100, Agilent) due to their surface plasmon resonance (λ_{max}, 519 nm) and by transmission electron microscopy (TEM, FEI Tecnai T20). A molar extinction coefficient (λ = 450) of 1.76 x 10^8 was used to determine the particles concentration (Haiss, Thanh et al. 2007). For AuNPs stabilization, a bifunctional poly(ethylene glycol) [SH-EG(8)-$(CH_2)_2$-COOH] (PEG) was used (Conde, Ambrosone et al. 2012). After an incubation time of 16 h at room temperature, the excess of PEG chains were removed by centrifugation at 14,000 *x g* for 30 min at 4 °C, thrice. Twenty pmol of AuNPs conjugated to PEG (AuNPs@PEG) were incubated with different amounts and ratios of EDC and sulfo-NHS [Fig. 39] in 1 mL of 10 mM 2-(N-morpholino)ethanesulfonic acid (MES), pH 6.1.

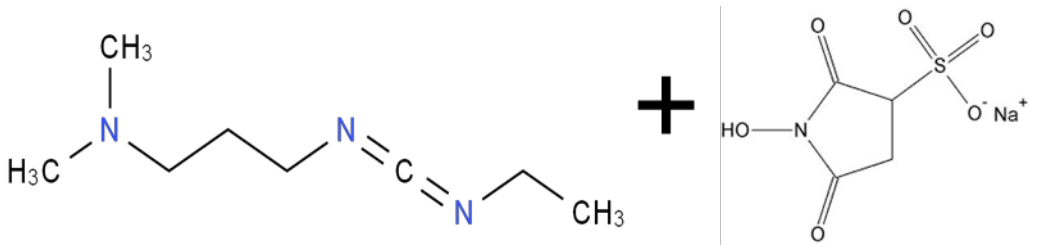

Figure 379 - Chemical structure of EDC (left) and sulfo-NHS (right).

After activation of PEG in the best condition to prevent the aggregation of AuNPs, different amounts of Esc(1-21) (from 1.5 to 4 µg) were added to the mixture and incubated at room temperature for 2 h. After removing the excess of unbound peptide by centrifugation as above, the stability of AuNPs conjugated with the peptide [AuNPs@Esc(1-21)] was assessed by UV-vis spectroscopy and the amount of 2 µg was chosen for all the experiments. The supernatant was recovered and analyzed for the amount of Esc(1-21) by the colorimetric microBCA protein assay reagent kit (Pierce, Rockford, IL), according to the manufacture instructions. ζ-potential was performed on a Malvern Zetasizer instrument at 25 °C.

6.4.4 - CS/PVA-Col nanoparticles and nano-embedded microparticles: synthesis and characterization

Col-loaded nanoparticles were prepared at 2% theoretical loading (2 mg of Col *per* 100 mg of NPs) by a modified emulsion/solvent diffusion technique (Ungaro, d'Angelo et al. 2012). A water in oil emulsion was achieved adding 100 µL of an aqueous Col solution (2 mg/ml) to 1 mL of PLGA-containing methylene chloride

(1% *w/v*) under vortex mixing (2400 min^{-1}, Heidolph, Germany). The emulsion was then added to 25 mL of an external diffusion phase leading to an immediate polymer precipitation in the form of NPs. The external diffusion phase was composed by an ethanol:water mixture (1:1 *v/v*) containing PVA (PVA/PLGA ratio 1:1 *w/w*) or CS (CS/PLGA ratio 1:20 *w/w*). The dispersion was kept under stirring at room temperature for 10 min; afterwards, residual organic solvent was evaporated under vacuum at 30 °C (Rotavapor®, Heidolph VV2000, Germany). NPs were isolated by centrifugation at 7000 rcf for 20 min at 4 °C and dispersed in ultrapure water. The morphology of obtained NPs was assessed by TEM.

Nano-embedded microparticles (NEM) were produced by co-spray drying Col-loaded NPs and an inert carrier (lactose) as follows: NPs were dispersed in an aqueous solution of lactose and then diluted with ethanol (ethanol/water ratio 1:1) up to a NPs concentration of 1 mg/mL and carrier concentration of 2% (*w/v*). The final dispersion was processed in a Mini Spray Dryer Büchi 190 (Flawil, Switzerland) equipped with a high-performance cyclone for the recovery of small powder amounts.

6.5 – ANTIMICROBIAL ACTIVITY

6.5.1 - Determination of the minimal growth inhibitory peptide concentration (MIC)

The antimicrobial activity of Esc(1-21) and [$Aib^{1,10,18}$]-Esc(1-21), was evaluated by performing the microbroth dilution assay in sterile 96-well plates, as outlined by the Clinical and Laboratory Standards Institute (2001), to determine the MIC. Serial 2-fold dilutions of peptide in 50 μL of Muller-Hinton (MH) broth were

prepared through the wells of the microtiter plate. Aliquots (50 µL) of bacteria at a concentration of $2x10^6$ (CFU)/mL in MH were added. MIC was defined as the lowest peptide concentration at which 100% inhibition of growth is visible after 16-18 h at 37°C. The same procedure was followed with yeasts in Winge medium (Valenti, Visca et al. 1985) using a final concentration of 3.5×10^4 CFU/mL and an incubation time of 18 h at 30 °C.

6.5.2 - Determination of the minimal bactericidal peptide concentration (MBC)

Bacteria were grown in LB broth at 37 °C till a mid-log phase which was aseptically monitored by absorbance at 590 nm (A_{590} = 0.8) with an UV-1700 Pharma Spec spectrophotometer (Shimadzu, Tokyo, Japan).

For the studies on Esc(1-21) and its diastereomer Esc(1-21)-1c, the minimal peptide concentration causing at least 99.9% bacterial killing was determined as follows: about 1×10^5 in 100 µL of PBS were incubated at 37 °C with the peptides in serial two-fold dilution. Aliquots (10 µL) were withdrawn after 30 min, diluted in LB and spread onto LB-agar plates. After overnight incubation, the number of CFU was counted.

Differently, for the experiments with AuNPs@Esc(1-21), the minimal peptide concentration causing at least 50% killing of bacteria (MBC_{50}) was determined. About 4×10^7 bacterial cells were incubated at 37 °C with serial twofold dilution of Esc(1-21), AuNPs@Esc(1-21) and AuNPs@PEG for 20 min. Aliquots were withdrawn and diluted in LB and spread onto LB-agar plates. After overnight incubation, the number of CFU was counted.

6.6 – PEPTIDE STABILITY TO PROTEOLYSIS

To evaluate the stability of Esc(1-21) (free or conjugated to AuNPs@PEG) to a proteolytic enzyme, i.e. trypsin, a concentration corresponding to 2 × MBC_{50} of the free peptide (2 μM) or AuNPs@Esc(1-21) (10 nM) in 100 mM sodium phosphate buffer (NaPB) was pre-incubated with trypsin (0.02 μg/mL) for 100 min at 37 °C under mild agitation in a volume of 50 μL. Afterwards, 50 μL of bacteria in NaPB were added to reach a final mixture volume of 100 μL and a cell density of about 4×10^8 CFU/mL in the presence of Esc(1-21) or AuNPs@Esc(1-21) at their MBC_{50} (1 μM and 5 nM, respectively). After 20 min treatment, aliquots were withdrawn and plated for counting.

6.7 – ANTIBIOFILM ACTIVITY

Biofilm formation was performed by adapting the procedure described in (Falciani, Lozzi et al. 2012), using the Calgary Biofilm Device (Innovotech, Innovotech Inc. Edmonton, Canada) as follows: 96-well plates, each well containing 150 μL of the bacterial inoculum (1×10^7 CFU/mL) in LB medium, were sealed with 96-pegs-lid on which biofilm can build up. The plates were then incubated for 20 h in a humidified incubator at 35 °C under agitation at 125 rpm. Each pegs-lid was rinsed twice with PBS and transferred to a "challenge plate" each well containing 200 μL of Esc(1-21), Esc(1-21)-1c, AuNPs@PEG or AuNPs@Esc(1-21) for 2 h. As reported in literature (Luca, Stringaro et al. 2013), three different assays can be performed to evaluate the antibiofilm activity of a drug: (i) absorbance measurement of reduced MTT; (ii) CFU counting; and (iii) crystal violet (CV) staining.

For the experiments with Esc(1-21) and its diastereomer, the antibiofilm activity was evaluated by determining the amount of viable biofilm cells. This was achieved by measuring the reduction of MTT to its insoluble formazan [Fig. 40]. MTT is a tetrazolium salt, which is reduced to an insoluble formazan product, by mitochondrial reductases, giving a purple color. The intensity of the color is directly proportional to the number of viable cells.

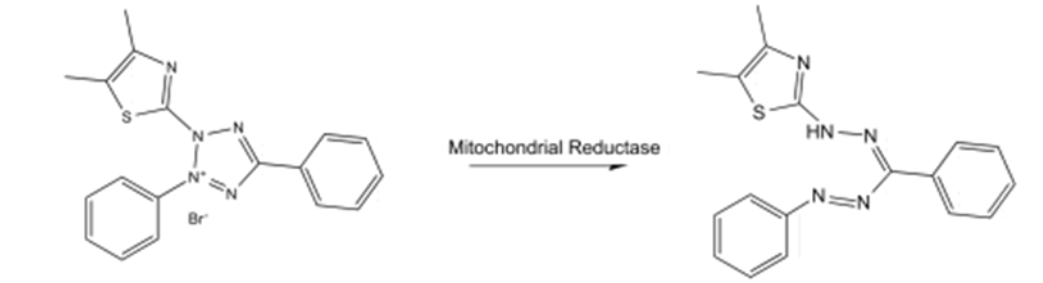

Figure 40 - Reduction of the yellow tetrazole to purple insoluble formazan, by metabolically-active cells.

After peptide treatment, the peg-lids were rinsed with PBS, transferred to another 96-wells plate, each well containing 1 mg/mL MTT, and incubated for 4 h at 37 °C. SDS (5 % final concentration) was then added to stop the reaction and to solubilize the formazan crystals. Bacterial viability was determined by absorbance measurements at 595 nm and calculated with respect to the control.

In the case of AuNPs@Esc(1-21), to avoid any possible interference on the absorbance of reduced MTT by the red color of AuNPs suspension, the antibiofilm activity was determined by CFU counts. The minimal biofilm eradication

concentration ($MBEC_{50}$) was defined as the lowest drug concentration sufficient to cause at least 50% killing of biofilm cells within 2 h. After peptide/AuNPs@Esc(1-21) treatment, pegs were washed with PBS, broken from the lid and transferred into eppendorf tubes containing 200 µL of PBS. Samples were sonicated three times for 10 min in an ultra-sonic water bath to detach bacterial cells from the pegs. Aliquots were withdrawn and spread onto LB-agar plates for colony counting.

Differently, with regards to CS/PVA-Col loaded nanoparticles, the effect on total biofilm biomass (viable cells plus extracellular matrix) was determined by the CV staining (Luca, Stringaro et al. 2013). In this case, after biofilm formation as described above, the peg-lids were rinsed twice with PBS and transferred into "challenge plates" each well containing 200 µL of free Col, Col-CS and Col-PVA NEM. The plates were then incubated for 24 h, 48 h and 72 h at 37 °C in a humidified incubator. Afterwards, the pegs were fixed in 99% methanol for 15 min at room temperature, and stained with CV solution (0.05% in water) for 15 min. Bound CV was released from pegs using 33% acetic acid. The absorbance was measured at 600 nm.

6.8 - MECHANISM OF ACTION: MEMBRANE PERMEABILIZATION ASSAYS

6.8.1 – *β-galactosidase assay*

The ability of Esc(1-21) and its diastereomer Esc(1-21)-1c to damage the cytoplasmic membrane of *P. aeruginosa* cells was determined by measuring the extracellular leakage of the cytosolic enzyme β-galactosidase, using ortho-Nitrophenyl-β-galactoside (ONPG) as a substrate (Marcellini, Borro et al. 2009) [Fig. 41]. *P. aeruginosa* PAO1, that constitutively expresses the β-galactosidase, was grown at 37 °C in LB till a mid-log phase, washed twice, centrifuged for 10 min (1,4 *x g*) and resuspended in 0.1 M NaPB at OD_{590} = 0.8 . About $1x10^6$ bacterial cells (in 100 µl NaPB) were incubated with two different concentrations of Esc(1-21) and Esc(1-21)-1c, i.e. 10 µM and 20 µM, for 30 min at 37 °C. Controls were bacteria without peptide, whereas the maximal membrane perturbation was obtained after treating bacteria with the highest peptide concentration used (20 µM) followed by the addition of 1 mM ethylenediaminetetraacetic acid (EDTA) + 0,5% Triton X-100 (final concentration) to completely destabilize the lipopolysaccharide outer membrane and to solubilize the phospholipid bilayer of the cytoplasmic membrane (Uccelletti, Zanni et al. 2010). At the end of the incubation time, aliquots were withdrawn, diluted in LB, and spread on LB plates for counting. Afterwards, 450 µL of NaPB were added to the remaining bacterial suspension, which was passed through a 0.2-µm filter. The hydrolysis of 2 mM ONPG, added to the culture filtrate, was recorded at 420 nm using a spectrophotometer (UV-1700 Pharma Spec Shimadzu).

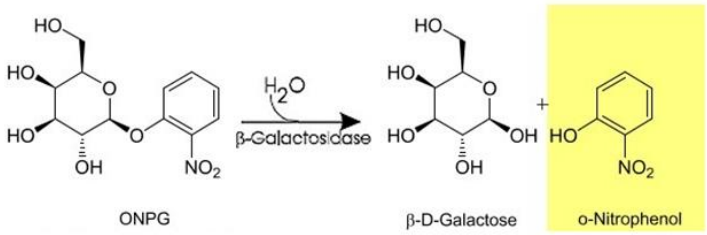

Figure 41 - β-galactosidase hydrolysis of the colorless ONPG to produce galactose and the yellow o-nitrophenol, which absorbs light at 420 nm.

6.8.2 – *Carboxyfluorescein leakage assay*

Peptide-membrane interaction can be investigated by the use of liposomes as model membranes, due to their bilayer structure, which is in principle identical to the lipid organization of biological membranes.

In the CF leakage assay, a concentration of lipid vesicles of 200 μM and different peptide concentrations of Esc(1-21) and Esc(1-21)-1c were used. After peptide addition, CF leakage from the damaged liposomes was recorded at λ_{em}=520 nm with λ_{exc}= 488 nm and monitored for 30 min. The percentage of CF released was calculated with respect to the control (untreated liposomes). A schematic representation of CF-encapsulated liposomes is shown in [Fig. 42].

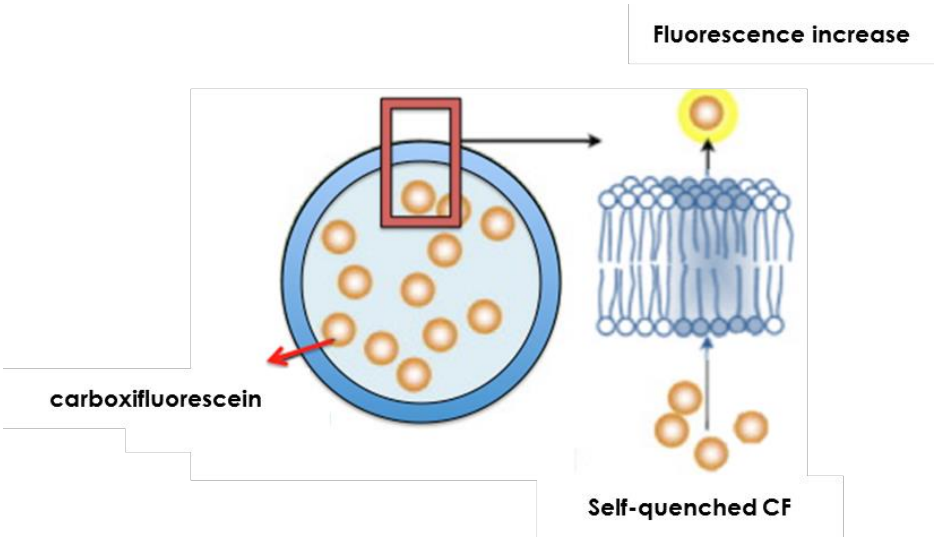

Figure 42 - Schematic representation of a CF-encapsulated liposome

6.8.3 – *Sytox Green assay*

The ability of AuNPs@Esc(1-21) to affect the membrane permeability of *P. aeruginosa* cells, was assessed by the Sytox Green assay in microtiter plates as previously described for the free peptide (Luca, Stringaro et al. 2013). Briefly, bacterial cells ($4x10^8$ CFU/mL) in NaPB supplemented with 1 μM Sytox Green [Fig. 43] were added to each well.

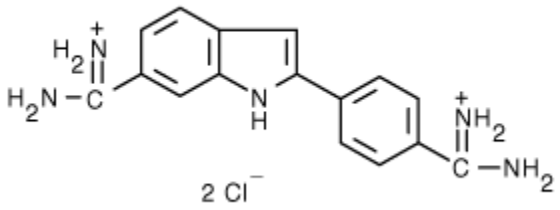

Figure 383 - Chemical structure of Sytox Green

Then, AuNPs@Esc(1-21), AuNPs@PEG or free Esc(1-21) were added at the indicated concentration. For the control sample, peptide solvent (water) was used. The increase in fluorescence, owing to the binding of the dye to intracellular DNA, was measured every min for 30 min at 37 °C with a microplate reader (Infinite M200; Tecan, Salzburg, Austria) at excitation and emission wavelengths equal to 485 and 535 nm, respectively. Final values were reported as ratio of each value (measured within 30 min) to the initial one measured after 1 min. Considering the absorbance of AuNPs@PEG as a background, the measurements of these samples were properly subtracted from those containing AuNPs@Esc(1-21).

6.9 – ELECTRON MICROSCOPY

To visualize the membrane-perturbing activity of AuNPs@Esc(1-21), SEM and TEM analysis were performed.

For SEM analysis, *P. aeruginosa* was grown overnight at 37 °C in LB. After 10 min centrifugation at 1400×*g*, the bacterial pellet was

resuspended in NaPB to an OD_{590} = 0.8. The bacterial culture was passed through a syringe to avoid possible clumps. Approximately 4 × 10^7 bacterial cells in a total volume of 100 µL were incubated with AuNPs@Esc(1-21) or AuNPs@PEG at 37 °C in a thermomixer under agitation for different times (1 min, 8 min and 15 min). Controls were buffer-treated bacterial cells. At the indicated time intervals, samples were centrifuged at 6000×*g* for 10 min and washed three times with NaPB. Afterwards, they were fixed with 2.5% glutaraldehyde (100 µL) in NaPB for 2 h at room temperature. The samples were then centrifuged at 12,000×*g* for 10 min and washed three times as above. Samples were analyzed using an Environmental scanning electron microscope (ESEM, Quanta FEG 250) with a wet scanning-transmission electron microscopy (wet-STEM) detector at high vacuum mode. Specimens were mounted in a Quantifoil® holey carbon film copper grids and examined with a working distance between 7 and 10 mm and an accelerating voltage of 20 kV.

For TEM analysis, bacterial samples were similarly prepared as described above but in a total volume of 1 mL. After washing and fixing cycles (as for SEM, but in a total volume of 1 mL), the pellets were subsequently embedded in 1.5% agar (Panreac); post fixed in 2% osmium tetroxide for 1 h at room temperature and stained in 1% uranyl acetate in the dark for 2 h at 4 °C. Then, they were rinsed in distilled water, dehydrated in ethanol and infiltrated overnight in Durcupan resin (Fluka). Following polymerization, embedded cultures were detached from the wells and

glued to araldite blocks. Finally, ultra-thin sections (0.08 μm) were cut with a diamond knife (Leica), stained with lead citrate (Reynolds solution) and examined under a 200 keV transmission electron microscope FEI Tecnai T20 (FEI Europe) operating at 60 keV.

6.10 - CYTOTOXICITY

The effect of Esc(1-21), [Aib^{1,10,18}]-Esc(1-21), Esc(1-21)-1c and AuNP@Esc(1-21) on the viability of mammalian cells was determined by the inhibition of MTT reduction to insoluble formazan by mitochondrial reductase. About 4 x 10^4 cells resuspended in the corresponding culture medium supplemented with glutamine, 2% FBS without antibiotics were plated in each well of a microtiter plate. After overnight incubation at 37 °C and 5% CO_2 atmosphere, the medium was replaced with fresh medium containing the peptides at different concentrations. The plates were then incubated for 2 or 24 h at 37 °C and 5% CO_2 atmosphere. After incubation time, the medium was removed and replaced with Hank's buffer containing 0.5 mg/mL MTT. After 4 h incubation, the formazan crystals were dissolved by adding acidified isopropanol. The viability was determined by absorbance measurements at 570 nm using a microplate reader reader (Infinite M200; Tecan, Salzburg, Austria). Cell viability was calculated with respect to the control according to the formula:

$$\frac{\text{Absorbance}_{\text{sample}} - \text{Absorbance}_{\text{blank}}}{\text{Absorbance}_{\text{control}} - \text{Absorbance}_{\text{blank}}} \times 100$$

where the blank is given by samples without cells and not treated with the peptides.

6.11 - CELL MIGRATION ASSAY

The ability of AuNPs@Esc(1-21) to stimulate migration of keratinocytes was studied according to a modified scratch assay (Di Grazia, Cappiello et al. 2015). Briefly, about 4 x 10^4 HaCaT cells suspended in DMEM supplemented with 4 mM glutamine (DMEMg) 10% FBS were seeded on each side of an ibidi culture insert for live cell analysis (Ibidi, Munich, Germany). Inserts were placed into wells of a 24-wells plate and incubated at 37 °C and 5% CO_2 to allow cells grow to confluence. Afterwards, inserts were carefully removed to create a cell-free area (pseudo-wound) of approximately 500 μm. Afterwards, 300 μL of DMEMg supplemented with AuNPs@Esc(1-21) or AuNPs@PEG or the free peptide, were added. Control samples were cells treated with DMEMg in the presence of peptide solvent (water). Cells were allowed to migrate for 9 h in an appropriate incubator, at 37°C and 5% CO_2. At different time intervals, fields of the pseudo-wound area were visualized under an inverted microscope (Olympus CKX41) at ×4 magnification and photographed with a Color View II digital camera. The percentage of cell-covered area at each time was determined by WIMASIS Image Analysis program.

6.12 – STATISTICAL ANALYSIS

Quantitative data were expressed as the mean ± SEM or SD. Statistical analysis was performed using Student's t test or two-way analysis of variance (ANOVA), with PRISM software (GraphPad, San Diego, CA). Differences were considered to be statistically significant for $p < 0.05$. The levels of statistical significance are indicated in the legend to figures.

7. References

Acuna, L., G. Picariello, et al. (2012). "A new hybrid bacteriocin, Ent35-MccV, displays antimicrobial activity against pathogenic Gram-positive and Gram-negative bacteria." FEBS Open Bio **2**: 12-19.

Afacan, N. J., A. T. Yeung, et al. (2012). "Therapeutic potential of host defense peptides in antibiotic-resistant infections." Curr Pharm Des **18**(6): 807-819.

Ageitos, J. M., A. Sanchez-Perez, et al. (2016). "Antimicrobial peptides (AMPs): Ancient compounds that represent novel weapons in the fight against bacteria." Biochem Pharmacol.

Ali, A., H. Zafar, et al. (2016). "Synthesis, characterization, applications, and challenges of iron oxide nanoparticles." Nanotechnol Sci Appl **9**: 49-67.

Andrushchenko, V. V., H. J. Vogel, et al. (2007). "Interactions of tryptophan-rich cathelicidin antimicrobial peptides with model membranes studied by differential scanning calorimetry." Biochim Biophys Acta **1768**(10): 2447-2458.

Bahar, A. A. and D. Ren (2013). "Antimicrobial peptides." Pharmaceuticals (Basel) **6**(12): 1543-1575.

Bellanda, M., E. Peggion, et al. (2001). "Conformational study of an Aib-rich peptide in DMSO by NMR." J Pept Res **57**(2): 97-106.

Boman, H. G. (1995). "Peptide antibiotics and their role in innate immunity." Annu Rev Immunol **13**: 61-92.

Bowdish, D. M., D. J. Davidson, et al. (2005). "Impact of LL-37 on anti-infective immunity." J Leukoc Biol **77**(4): 451-459.

Bowdish, D. M. and R. E. Hancock (2005). "Anti-endotoxin properties of cationic host defence peptides and proteins." J Endotoxin Res **11**(4): 230-236.

Brogden, K. A. (2005). "Antimicrobial peptides: pore formers or metabolic inhibitors in bacteria?" Nat Rev Microbiol **3**(3): 238-250.

Brogden, K. A., M. Ackermann, et al. (2003). "Antimicrobial peptides in animals and their role in host defences." Int J Antimicrob Agents **22**(5): 465-478.

Brogden, N. K. and K. A. Brogden (2011). "Will new generations of modified antimicrobial peptides improve their potential as pharmaceuticals?" Int J Antimicrob Agents **38**(3): 217-225.

Cabuzu, D., A. Cirja, et al. (2015). "Biomedical applications of gold nanoparticles." Curr Top Med Chem **15**(16): 1605-1613.
Chan, D. I., E. J. Prenner, et al. (2006). "Tryptophan- and arginine-rich antimicrobial peptides: structures and mechanisms of action." Biochim Biophys Acta **1758**(9): 1184-1202.
Chatterjee, S., A. Bandyopadhyay, et al. (2011). "Effect of iron oxide and gold nanoparticles on bacterial growth leading towards biological application." J Nanobiotechnology **9**: 34.
Conde, J., A. Ambrosone, et al. (2012). "Design of multifunctional gold nanoparticles for in vitro and in vivo gene silencing." ACS Nano **6**(9): 8316-8324.
Conlon, J. M. (2011). "Structural diversity and species distribution of host-defense peptides in frog skin secretions." Cell Mol Life Sci **68**(13): 2303-2315.
Connor, E. E., J. Mwamuka, et al. (2005). "Gold nanoparticles are taken up by human cells but do not cause acute cytotoxicity." Small **1**(3): 325-327.
d'Angelo, I., C. Conte, et al. (2014). "Improving the efficacy of inhaled drugs in cystic fibrosis: challenges and emerging drug delivery strategies." Adv Drug Deliv Rev **75**: 92-111.
d'Angelo, I., C. Conte, et al. (2015). "Pulmonary drug delivery: a role for polymeric nanoparticles?" Curr Top Med Chem **15**(4): 386-400.
d'Angelo, I., F. Quaglia, et al. (2015). "PLGA carriers for inhalation: where do we stand, where are we headed?" Ther Deliv **6**(10): 1139-1144.
Dathe, M., T. Wieprecht, et al. (1997). "Hydrophobicity, hydrophobic moment and angle subtended by charged residues modulate antibacterial and haemolytic activity of amphipathic helical peptides." FEBS Lett **403**(2): 208-212.
Davidson, D. J., A. J. Currie, et al. (2004). "The cationic antimicrobial peptide LL-37 modulates dendritic cell differentiation and dendritic cell-induced T cell polarization." J Immunol **172**(2): 1146-1156.
De Zotti, M., B. Biondi, et al. (2012). "Antimicrobial lipopeptaibol trichogin GA IV: role of the three Aib residues on conformation and bioactivity." Amino Acids **43**(4): 1761-1777.
Di Grazia, A., F. Cappiello, et al. (2015). "The frog skin-derived antimicrobial peptide esculentin-1a(1-21)NH_2 promotes the migration of human HaCaT keratinocytes in an EGF receptor-dependent manner: a novel promoter of human skin wound healing?" PLoS One **10**(6): e0128663.

Ehrenstein, G. and H. Lecar (1977). "Electrically gated ionic channels in lipid bilayers." Q Rev Biophys **10**(1): 1-34.
Falciani, C., L. Lozzi, et al. (2012). "Isomerization of an antimicrobial peptide broadens antimicrobial spectrum to gram-positive bacterial pathogens." PLoS One **7**(10): e46259.
Fernandez-Vidal, M., S. Jayasinghe, et al. (2007). "Folding amphipathic helices into membranes: amphiphilicity trumps hydrophobicity." J Mol Biol **370**(3): 459-470.
Fjell, C. D., J. A. Hiss, et al. (2012). "Designing antimicrobial peptides: form follows function." Nat Rev Drug Discov **11**(1): 37-51.
Flemming, H. C., J. Wingender, et al. (2016). "Biofilms: an emergent form of bacterial life." Nat Rev Microbiol **14**(9): 563-575.
Gazit, E., W. J. Lee, et al. (1994). "Mode of action of the antibacterial cecropin B2: a spectrofluorometric study." Biochemistry **33**(35): 10681-10692.
Gellatly, S. L. and R. E. Hancock (2013). "*Pseudomonas aeruginosa*: new insights into pathogenesis and host defenses." Pathog Dis **67**(3): 159-173.
Giangaspero, A., L. Sandri, et al. (2001). "Amphipathic alpha helical antimicrobial peptides." Eur J Biochem **268**(21): 5589-5600.
Giuliani, A. and A. C. Rinaldi (2011). "Beyond natural antimicrobial peptides: multimeric peptides and other peptidomimetic approaches." Cell Mol Life Sci **68**(13): 2255-2266.
Goblyos, A., K. J. Schimmel, et al. (2013). "Development of a nose cream containing the synthetic antimicrobial peptide P60.4Ac for eradication of methicillin-resistant *Staphylococcus aureus* carriage." J Pharm Sci **102**(10): 3539-3544.
Greish, K., G. Thiagarajan, et al. (2012). "Size and surface charge significantly influence the toxicity of silica and dendritic nanoparticles." Nanotoxicology **6**(7): 713-723.
Grieco, P., A. Carotenuto, et al. (2013). "The effect of d-amino acid substitution on the selectivity of temporin L towards target cells: identification of a potent anti-*Candida* peptide." Biochim Biophys Acta **1828**(2): 652-660.
Gupta, M. and V. S. Chauhan (2011). "*De novo* design of alpha,beta-didehydrophenylalanine containing peptides: from models to applications." Biopolymers **95**(3): 161-173.

Gutjahr, A., C. Phelip, et al. (2016). "Biodegradable polymeric nanoparticles-based vaccine adjuvants for lymph nodes targeting." Vaccines (Basel) **4**(4).

Haiss, W., N. T. Thanh, et al. (2007). "Determination of size and concentration of gold nanoparticles from UV-vis spectra." Anal Chem **79**(11): 4215-4221.

Hall, K. and M. I. Aguilar (2010). "Surface plasmon resonance spectroscopy for studying the membrane binding of antimicrobial peptides." Methods Mol Biol **627**: 213-223.

Hancock, R. E. and H. G. Sahl (2006). "Antimicrobial and host-defense peptides as new anti-infective therapeutic strategies." Nat Biotechnol **24**(12): 1551-1557.

Haslam, I. S., E. W. Roubos, et al. (2014). "From frog integument to human skin: dermatological perspectives from frog skin biology." Biol Rev Camb Philos Soc **89**(3): 618-655.

Hemshekhar, M., V. Anaparti, et al. (2016). "Functions of cationic host defense peptides in immunity." Pharmaceuticals (Basel) **9**(3).

Hong, S. Y., J. E. Oh, et al. (1999). "Effect of D-amino acid substitution on the stability, the secondary structure, and the activity of membrane-active peptide." Biochem Pharmacol **58**(11): 1775-1780.

Huang, Y., J. Huang, et al. (2010). "Alpha-helical cationic antimicrobial peptides: relationships of structure and function." Protein Cell **1**(2): 143-152.

Islas-Rodriguez, A. E., L. Marcellini, et al. (2009). "Esculentin 1-21: a linear antimicrobial peptide from frog skin with inhibitory effect on bovine mastitis-causing bacteria." J Pept Sci **15**(9): 607-614.

Ivanov, M. R., H. R. Bednar, et al. (2009). "Investigations of the mechanism of gold nanoparticle stability and surface functionalization in capillary electrophoresis." ACS Nano **3**(2): 386-394.

Jenssen, H. (2009). "Therapeutic approaches using host defence peptides to tackle herpes virus infections." Viruses **1**(3): 939-964.

Jiang, Z., A. I. Vasil, et al. (2009). "Effects of net charge and the number of positively charged residues on the biological activity of amphipathic alpha-helical cationic antimicrobial peptides." Adv Exp Med Biol **611**: 561-562.

Kim, J. Y., S. C. Park, et al. (2011). "C-terminal amidation of PMAP-23: translocation to the inner membrane of Gram-negative bacteria." Amino Acids **40**(1): 183-195.

Kolar, S. S., V. Luca, et al. (2015). "Esculentin-1a(1-21)NH_2: a frog skin-derived peptide for microbial keratitis." Cell Mol Life Sci **72**(3): 617-627.

Konig, E., O. R. Bininda-Emonds, et al. (2015). "The diversity and evolution of anuran skin peptides." Peptides **63**: 96-117.

Ladram, A. and P. Nicolas (2016). "Antimicrobial peptides from frog skin: biodiversity and therapeutic promises." Front Biosci (Landmark Ed) **21**: 1341-1371.

Lee, D. G., H. N. Kim, et al. (2002). "Design of novel analogue peptides with potent antibiotic activity based on the antimicrobial peptide, HP (2-20), derived from N-terminus of *Helicobacter pylori* ribosomal protein L1." Biochim Biophys Acta **1598**(1-2): 185-194.

Liu, L., Y. Fang, et al. (2011). "A rigidity-enhanced antimicrobial activity: a case for linear cationic alpha-helical peptide HP(2-20) and its four analogues." PLoS One **6**(1): e16441.

Luca, V., A. Stringaro, et al. (2013). "Esculentin(1-21), an amphibian skin membrane-active peptide with potent activity on both planktonic and biofilm cells of the bacterial pathogen *Pseudomonas aeruginosa*." Cell Mol Life Sci **70**(15): 2773-2786.

Lyczak, J. B., C. L. Cannon, et al. (2000). "Establishment of *Pseudomonas aeruginosa* infection: lessons from a versatile opportunist." Microbes Infect **2**(9): 1051-1060.

Ma, B., C. Niu, et al. (2016). "The disulfide bond of the peptide Thanatin is dispensible for its antimicrobial activity *In Vivo* and *In Vitro*." Antimicrob Agents Chemother **60**(7): 4283-4289.

Mangoni, M. L., D. Fiocco, et al. (2003). "Functional characterisation of the 1-18 fragment of esculentin-1b, an antimicrobial peptide from *Rana esculenta*." Peptides **24**(11): 1771-1777.

Mangoni, M. L., R. Miele, et al. (2001). "The synthesis of antimicrobial peptides in the skin of *Rana esculenta* is stimulated by microorganisms." FASEB J **15**(8): 1431-1432.

Mangoni, M. L., N. Papo, et al. (2006). "Effect of natural L- to D-amino acid conversion on the organization, membrane binding, and biological function of the antimicrobial peptides bombinins H." Biochemistry **45**(13): 4266-4276.

Manning, M. C. and R. W. Woody (1991). "Theoretical CD studies of polypeptide helices: examination of important electronic and geometric factors." Biopolymers **31**(5): 569-586.

Marcellini, L., M. Borro, et al. (2009). "Esculentin-1b(1-18)--a membrane-active antimicrobial peptide that synergizes with antibiotics and modifies the expression level of a limited number of proteins in *Escherichia coli*." FEBS J **276**(19): 5647-5664.

Melo, M. N., D. Dugourd, et al. (2006). "Omiganan pentahydrochloride in the front line of clinical applications of antimicrobial peptides." Recent Pat Antiinfect Drug Discov **1**(2): 201-207.

Mookherjee, N. and R. E. Hancock (2007). "Cationic host defence peptides: innate immune regulatory peptides as a novel approach for treating infections." Cell Mol Life Sci **64**(7-8): 922-933.

Mouritsen, O. G. (2011). "Model answers to lipid membrane questions." Cold Spring Harb Perspect Biol **3**(9): a004622.

Nakatsuji, T. and R. L. Gallo (2012). "Antimicrobial peptides: old molecules with new ideas." J Invest Dermatol **132**(3 Pt 2): 887-895.

Neville, F., M. Cahuzac, et al. (2006). "Lipid headgroup discrimination by antimicrobial peptide LL-37: insight into mechanism of action." Biophys J **90**(4): 1275-1287.

Nguyen, L. T., E. F. Haney, et al. (2011). "The expanding scope of antimicrobial peptide structures and their modes of action." Trends Biotechnol **29**(9): 464-472.

Nicolas, P. and C. El Amri (2009). "The dermaseptin superfamily: a gene-based combinatorial library of antimicrobial peptides." Biochim Biophys Acta **1788**(8): 1537-1550.

Nilsson, A. C., H. Janson, et al. (2015). "LTX-109 is a novel agent for nasal decolonization of methicillin-resistant and -sensitive *Staphylococcus aureus*." Antimicrob Agents Chemother **59**(1): 145-151.

Oren, Z. and Y. Shai (1997). "Selective lysis of bacteria but not mammalian cells by diastereomers of melittin: structure-function study." Biochemistry **36**(7): 1826-1835.

Paquette, D. W., D. M. Simpson, et al. (2002). "Safety and clinical effects of topical histatin gels in humans with experimental gingivitis." J Clin Periodontol **29**(12): 1051-1058.

Park, Y., S. C. Park, et al. (2007). "Structure-activity relationship of HP (2-20) analog peptide: enhanced antimicrobial activity by N-terminal random coil region deletion." Biopolymers **88**(2): 199-207.

Pasupuleti, M., A. Schmidtchen, et al. (2012). "Antimicrobial peptides: key components of the innate immune system." Crit Rev Biotechnol **32**(2): 143-171.

Pietro, P. D., G. Strano, et al. (2016). "Gold and silver nanoparticles for applications in theranostics." Curr Top Med Chem **16**(27): 3069-3102.

Powers, J. P. and R. E. Hancock (2003). "The relationship between peptide structure and antibacterial activity." Peptides **24**(11): 1681-1691.

Rai, A., S. Pinto, et al. (2016). "One-step synthesis of high-density peptide-conjugated gold nanoparticles with antimicrobial efficacy in a systemic infection model." Biomaterials **85**: 99-110.

Ramesh, S., M. Grijalva, et al. (2016). "Peptides conjugated to silver nanoparticles in biomedicine - a "value-added" phenomenon." Biomater Sci.

Rampioni, G., F. Polticelli, et al. (2007). "The *Pseudomonas* quorum-sensing regulator RsaL belongs to the tetrahelical superclass of H-T-H proteins." J Bacteriol **189**(5): 1922-1930.

Rampioni, G., M. Schuster, et al. (2007). "RsaL provides quorum sensing homeostasis and functions as a global regulator of gene expression in Pseudomonas aeruginosa." Mol Microbiol **66**(6): 1557-1565.

Reznickova, A., Z. Novotna, et al. (2015). "Gold, silver and carbon nanoparticles grafted on activated polymers for biomedical applications." J Nanosci Nanotechnol **15**(12): 10053-10073.

Rink, R., A. Arkema-Meter, et al. (2010). "To protect peptide pharmaceuticals against peptidases." J Pharmacol Toxicol Methods **61**(2): 210-218.

Sato, H. and J. B. Feix (2006). "Peptide-membrane interactions and mechanisms of membrane destruction by amphipathic alpha-helical antimicrobial peptides." Biochim Biophys Acta **1758**(9): 1245-1256.

Sengupta, D., H. Leontiadou, et al. (2008). "Toroidal pores formed by antimicrobial peptides show significant disorder." Biochim Biophys Acta **1778**(10): 2308-2317.

Shai, Y. (2002). "Mode of action of membrane active antimicrobial peptides." Biopolymers **66**(4): 236-248.

Shai, Y. and Z. Oren (1996). "Diastereoisomers of cytolysins, a novel class of potent antibacterial peptides." J Biol Chem **271**(13): 7305-7308.

Simmaco, M., G. Mignogna, et al. (1993). "Novel antimicrobial peptides from skin secretion of the European frog Rana esculenta." FEBS Lett **324**(2): 159-161.

Simmaco, M., G. Mignogna, et al. (1994). "Antimicrobial peptides from skin secretions of *Rana esculenta*. Molecular cloning of cDNAs

encoding esculentin and brevinins and isolation of new active peptides." J Biol Chem **269**(16): 11956-11961.
Soica, C., D. Coricovac, et al. (2016). "Nanocarriers as tools in delivering active compounds for immune system related pathologies." Recent Pat Nanotechnol **10**(2): 128-145.
Spudy, B., F. D. Sonnichsen, et al. (2012). "Identification of structural traits that increase the antimicrobial activity of a chimeric peptide of human beta-defensins 2 and 3." Biochem Biophys Res Commun **427**(1): 207-211.
Stella, L., C. Mazzuca, et al. (2004). "Aggregation and water-membrane partition as major determinants of the activity of the antibiotic peptide trichogin GA IV." Biophys J **86**(2): 936-945.
Stewart, J. C. (1980). "Colorimetric determination of phospholipids with ammonium ferrothiocyanate." Anal Biochem **104**(1): 10-14.
Strahilevitz, J., A. Mor, et al. (1994). "Spectrum of antimicrobial activity and assembly of dermaseptin-b and its precursor form in phospholipid membranes." Biochemistry **33**(36): 10951-10960.
Streeter, K., C. Neuman, et al. (2016). "The characteristics of genetically related *Pseudomonas aeruginosa* from diverse sources and their interaction with human cell lines." Can J Microbiol **62**(3): 233-240.
Subbalakshmi, C., R. Nagaraj, et al. (1999). "Biological activities of C-terminal 15-residue synthetic fragment of melittin: design of an analog with improved antibacterial activity." FEBS Lett **448**(1): 62-66.
Taylor, K., P. E. Barran, et al. (2008). "Structure-activity relationships in beta-defensin peptides." Biopolymers **90**(1): 1-7.
Thaiss, C. A., M. Levy, et al. (2016). "Integration of Innate Immune Signaling." Trends Immunol **37**(2): 84-101.
Toniolo, C., C. Peggion, et al. (1994). "Structure determination of racemic trichogin A IV using centrosymmetric crystals." Nat Struct Biol **1**(12): 908-914.
Torino, D., A. Mollica, et al. (2010). "Synthesis and evaluation of new endomorphin-2 analogues containing (Z)-alpha,beta-didehydrophenylalanine (Delta(Z)Phe) residues." J Med Chem **53**(11): 4550-4554.
Tsai, D. H., Y. F. Lu, et al. (2015). "Orthogonal analysis of functional gold nanoparticles for biomedical applications." Anal Bioanal Chem **407**(28): 8411-8422.
Uccelletti, D., E. Zanni, et al. (2010). "Anti-*Pseudomonas* activity of frog skin antimicrobial peptides in a *Caenorhabditis elegans* infection

model: a plausible mode of action *in vitro* and *in vivo*." Antimicrob Agents Chemother **54**(9): 3853-3860.
Ungaro, F., I. d'Angelo, et al. (2012). "Dry powders based on PLGA nanoparticles for pulmonary delivery of antibiotics: modulation of encapsulation efficiency, release rate and lung deposition pattern by hydrophilic polymers." J Control Release **157**(1): 149-159.
Uttley, L., S. Harnan, et al. (2013). "Systematic review of the dry powder inhalers colistimethate sodium and tobramycin in cystic fibrosis." Eur Respir Rev **22**(130): 476-486.
Valenti, P., P. Visca, et al. (1985). "Antifungal activity of ovotransferrin towards genus *Candida*." Mycopathologia **89**(3): 169-175.
Velden, W. J., T. M. van Iersel, et al. (2009). "Safety and tolerability of the antimicrobial peptide human lactoferrin 1-11 (hLF1-11)." BMC Med **7**: 44.
Wang, Y., Y. Zhang, et al. (2016). "Novel peptides from skins of amphibians showed broad-spectrum antimicrobial activities." Chem Biol Drug Des **87**(3): 419-424.
Weinstock, M. T., J. N. Francis, et al. (2012). "Protease-resistant peptide design-empowering nature's fragile warriors against HIV." Biopolymers **98**(5): 431-442.
Williams, D. N., S. H. Ehrman, et al. (2006). "Evaluation of the microbial growth response to inorganic nanoparticles." J Nanobiotechnology **4**: 3.
Wu, W. K., C. C. Wong, et al. (2010). "Cathelicidins in inflammation and tissue repair: Potential therapeutic applications for gastrointestinal disorders." Acta Pharmacol Sin **31**(9): 1118-1122.
Yih, T. C. and M. Al-Fandi (2006). "Engineered nanoparticles as precise drug delivery systems." J Cell Biochem **97**(6): 1184-1190.
Zelezetsky, I. and A. Tossi (2006). "Alpha-helical antimicrobial peptides--using a sequence template to guide structure-activity relationship studies." Biochim Biophys Acta **1758**(9): 1436-1449.
Zhang, L., R. Benz, et al. (1999). "Influence of proline residues on the antibacterial and synergistic activities of alpha-helical peptides." Biochemistry **38**(25): 8102-8111.
Zhang, L., A. Rozek, et al. (2001). "Interaction of cationic antimicrobial peptides with model membranes." J Biol Chem **276**(38): 35714-35722.

Zhang, Y., T. P. Shareena Dasari, et al. (2015). "Antimicrobial activity of gold nanoparticles and ionic gold." J Environ Sci Health C Environ Carcinog Ecotoxicol Rev **33**(3): 286-327.

8. Acknowledgments

The experimental work was performed under the supervision of Prof. Maria Luisa Mangoni, to whom I give my best thanks for her constant commitment and encouragement. Her valuable advice and her passion for scientific research have allowed me to grow both professionally and personally.

I am very grateful to all members of our lab group (Vincenzo, Mary, Floriana, Antonio, Marica, Gina, Olfa) who have collaborated with me and have created a friendly atmosphere.

I would like to thank all the collaborators:
Dr. Marco Crisma and Dr. Barbara Biondi at the "Institute of Biomolecular Chemistry, Padova Unit, CNR" for their valuable contribution in the design of the Aib-analog of Esc(1-21) and its structural characterization.
Prof. Anirban Bhunia, (Bose Institute, Kolkata, India), for the spectroscopic analysis of Esc(1-21) and Esc(1-21)-1c.
Prof. Alessandro Pini (Department of Medical Biotechnology, University of Siena) for the peptides' stability experiments.

The group of Instituto de Ciencia de Materiales de Aragon-CSIC/Universidad de Zaragoza, Spain who welcomed me with enthusiasm. In particular, my best thanks to Dr. Jesus de la Fuentes, Dr. Maria Moros and Sara Rivera-Fernàndez for their willingness and the precious advice during my stay in Spain, necessary to the preparation of gold nanoparticles.

Prof. Francesca Ungaro, Dr. Ivana d'Angelo and Prof. Fabiana Quaglia, at University "Federico II" (Naples), for making available their knowledge for the preparation of polymeric nanoparticles.

Prof. Lorenzo Stella (University of Tor Vergata, Rome) for the supervision during the preparation of model membranes, which were used for the studies on the mechanism of action of antimicrobial peptides.

Dr. Laura Mancini and Dr. Stefania Marcheggiani (Istituto Superiore di Sanità, Roma) for having made available the space for microbiological research.

Appendix: reprint of the papers